

Article citation info:

Ye Y, Xiong C, Ma B, Zhou Q, Yu L, Hybrid reliability analysis method for systems with random and non-parameterized p-boxes based on weight coefficients, *Eksploracja i Niezawodność – Maintenance and Reliability* 2024: 26(4) <http://doi.org/10.17531/ein/191458>

Hybrid reliability analysis method for systems with random and non-parameterized p-boxes based on weight coefficients

Indexed by:



Yan Ye^a, Cenbo Xiong^{a,*}, Biao Ma^a, Qinghua Zhou^b, Liang Yu^a

^a School of Mechanical Engineering, Beijing Institute of Technology, China

^b School of Aeronautics and Astronautics, Sichuan University, China

Highlights

- Based on discrete intervals and important samples, the interval weights of samples are established to describe the distribution characteristics of probability boxes (p-boxes) variables better.
- Combining the Monte Carlo method (MCS) and interval weights, a more efficient failure probability optimization model is constructed.
- The boundaries fitted by the optimal weights are more reasonable than the ones yielded by Interval Monte Carlo (IMCS).

Abstract

This paper establishes a hybrid variable system failure probability optimization model based on sampling methods and weighting coefficients. By introducing auxiliary input variables, important sampling functions, and p-box, failure samples are mapped from the random variable space to the p-box variable space. The new weight coefficients are constructed, including important sampling weights and interval weights. Combining discretization methods and Monte Carlo simulation (MCS), the interval weights are transformed into variables, and constraints conforming to the p-box variable distribution are constructed. After calculating the weighting coefficients for all failure samples, the new failure probability optimization model is built. This model is independent of the performance functions and does not involve cyclic optimization, with computational complexity only related to the dimensions. Six cases are used for method comparison, validating that the new method exhibits higher efficiency and accuracy.

Keywords

hybrid reliability analysis, Non-Parameterized p-boxes; weight coefficients, optimizing equation

This is an open access article under the CC BY license (<https://creativecommons.org/licenses/by/4.0/>)

1. Introduction

In practical engineering, the factors influencing structural performance and security are frequently subject to inaccuracies. Many of these factors involve uncertainties, which introduce both epistemic uncertainty (lack of knowledge) and aleatory uncertainty (natural variability)[25, 34]. Therefore, conducting reliability analysis on systems with uncertain variables is a critical task in engineering.

The conventional approach to dealing with uncertain parameters is through the probability model, where the probability distributions of the uncertain parameters are

explicitly defined using available information. In fact, obtaining complete information and accurately determining the probability distribution of the uncertain parameters is challenging. This limitation constitutes the primary drawback of these probability-based methods.

Furthermore, some available tools to describe the epistemic variables are often mentioned, such as Bayesian approaches[6, 12, 39], interval probabilities[22, 23, 38], fuzzy sets[40, 48], info-gap theory[2, 14], evidence theory[11, 32] and probability boxes[17, 18, 24]. Specifically, Bayesian approaches and fuzzy

(*) Corresponding author.

E-mail addresses:

Y. Ye (ORCID: 0009-0003-2228-7786) yeyanzzz@163.com, C. Xiong xiongyi1895@163.com, B. Ma mabiao@bit.edu.cn, Q. Zhou qh.zhou@foxmail.com, L. Yu yuliang0516@126.com,

sets focus on acquiring information to establish prior distributions and membership functions. Evidence theory and interval probabilities are effective in handling fragmented information. The interval model is part of the info-gap theory, allowing for the consideration of inadequately described structures. In this case, uncertain parameters are quantified using change bounds as opposed to exact probability distributions.

Probability boxes combine the advantages of probability and interval models, allowing for the consideration of both randomness and imprecision simultaneously. A p-box quantifies uncertainty using a pair of lower and upper cumulative distribution functions (CDFs). It restricts the distribution of epistemic variables to a specific range without requiring precise assumptions. In this paper, the variables are modeled by probability boxes that account for both aleatory and epistemic uncertainty. The p-box can be further classified into parameterized and non-parameterized (free) representations. Several approaches have been utilized to analyze the reliability of parametric p-boxes[18-20, 33]. Free p-boxes are a more general form, and various methods have been proposed for their analysis in recent years[9, 16, 29, 30, 37, 45, 46].

The conventional approach to handling p-box variables is through the Cartesian product method (CPM)[5]. However, the computational complexity of the CPM increases exponentially with the number of dimensions. Furthermore, a combination of line sampling and imprecise probabilities, which shows high efficiency in the cases with moderate non-linearities, was discussed by Angelis et al[7].

With the development of the sampling technique, the application of Monte Carlo simulation (MCS)[43, 44] become popular in hybrid reliability analysis under both random and p-box variables (HRA-RP)[31]. Double-Loop Sampling (DLS)[26] and Interval Monte Carlo (IMCS)[45] were proposed by Recuk et al and Zhang et al, respectively. DLS contains two layers of sampling, the outer layer samples the distribution parameters, and the inner layer samples the extracted probability distribution to calculate the failure probability. In IMCS, it gained samples of random variables and intervals of p-box variables by inverse transformation method, and calculated the extreme values over these samples and intervals. However, it was hard to deal with complex explicit performance functions

and implicit performance function. Interval importance sampling[43] and interval quasi-MCS method[44] were proposed to solve the small failure problem and improve the efficiency of IMCS. On this basis, to decrease the number of performance function evaluations, surrogate models are considered, including polynomial response surface[10], support vector machine[28], neural networks[26], and Kriging[6, 35, 41, 42]. Kriging is widely used because of its advantages. Thus, the method named Active Learning Kriging And Optimization-based Interval Monte Carlo Simulation (ALK-OIMCS), and the method named Bounding-limit-state-surfaces-based Active Learning Kriging and IMCS (BLSK-IMCS) were proposed by Yang et al[38] and Zhang et al[46], respectively. They used some optimization algorithms[1, 3, 13, 15] to improve the accuracy of the model. The process of obtaining sample intervals in ALK-OIMCS and BLSK-IMCS is similar to IMCS, but the difference lies in the learning functions.

Diego et al[4] combined subset simulation with random set theory to calculate the lower and upper bounds of failure probability. It samples a series of points from random sets, calculates the boundary of failure probability and utilizes subset simulation to do further calculations. Liu et al[21] transform the original uncertain space into the standard normal space and establish two two-layer nesting optimization models to solve the extremum. Schöbi and Sudret[29] proposed imprecise structural reliability analysis (ISRA) based on multi-level metamodels[47]. The first level aims to approximate the performance function, and the second level included two independent Kriging metamodels are used to calculate the boundaries. Li et al [16] proposed an uncertainty propagation method based on the discretization of the cumulative distribution function, calculated the value range of the first four statistical moments of the response probability box, and used Johnson distribution fitting and percentage optimization to construct the boundary distribution of the response probability box. A collaborative interval quasi-Monte Carlo method (CIMCM) is presented by Xiao et al[49]. Rosen's gradient projection method (RGPM) is utilized to solve the extreme values, and the number of repeated search iterations is reduced. A linear programming model, which is constructed by discrete CDF and used to solve the failure probability boundary, is proposed by Xie et al[36]. It solves the univariate problem by constructing linear constraints

and decomposes the multivariable problem into a series of single-variable problems by using iterative techniques.

Accounting for all of them, the idea of finding extremums on intervals is similar. They assume that p-box variables have unrestricted distribution between the lower and upper CDFs, disregarding that the CDF of the p-box variable follows the rule of general CDF. Consequently, this perspective results in inaccurate estimations of the upper and lower bounds of failure probability. The method proposed by Xie et al[36] solves the reasonable constraint problem of univariate problems and compares it with IMCS. But it does not delve into the difference between itself and IMCS. At the same time, the method needs to call the function repeatedly to calculate the conditional failure probability in the process of iterative optimization, which reduces the computational efficiency.

In order to obtain more reasonable failure probability boundary accurately and simplify the solving process, this paper proposes a novel approach that utilizes a newly constructed weight coefficient. The main idea is to use auxiliary input functions, important sampling functions, and p-box probability density functions to map failure samples from the random space to the p-box variable space. Combining discretization methods to assign interval weights to the samples and treating them as variables to construct optimization equations. This approach not only aligns with the characteristics of p-box CDFs but also guarantees accuracy. The upper and lower bounds of failure probability are determined through the computation of an optimal solution. In addition, the performance of this method is tested by six case studies and compared with IMCS and the method proposed by Xie. The findings demonstrate that the proposed method is both accurate and effective in the domain of HRA-RP.

The rest of this article is outlined as follows. The characteristics of p-box variables, the IMCS, and its shortcomings are introduced in Section 2. Section 3 introduces the construction of the weight coefficient and optimization function of the proposed method. In Section 4, six cases studies are conducted to analyze the three methods. We make a conclusion in Section 5.

2. Hybrid Reliability Analysis with Both Random and P-box Variables

2.1. P-box Variables and Hybrid Reliability Analysis

The p-box variable is constructed by a pair of upper and lower limit cumulative distribution functions. When the cumulative distribution function of the P-box variable \mathbf{P} is defined as $F_{\mathbf{P}}(\mathbf{p})$, the p-box variable is expressed as

$$\underline{F}_{\mathbf{P}}(\mathbf{p}) \leq F_{\mathbf{P}}(\mathbf{p}) \leq \bar{F}_{\mathbf{P}}(\mathbf{p}), \quad (1)$$

where \mathbf{p} is a realization of \mathbf{P} , $\underline{F}_{\mathbf{P}}(\mathbf{p})$ and $\bar{F}_{\mathbf{P}}(\mathbf{p})$ are the lower and upper CDFs respectively.

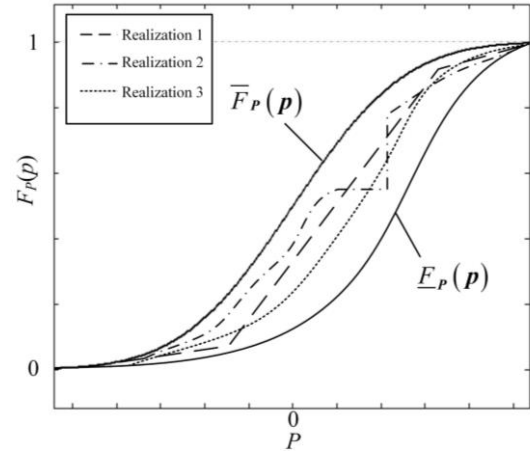


Fig. 1. Boundary curves of free p-box and realizations of the true but unknown CDF.

Free p-box is only defined by Eq. (1), and it means that the free p-box can have any shape in the restricted region as long as it conforms to the characteristics of the cumulative distribution function. Fig. 1 shows some possible shapes of free p-box, such as piecewise functions (Realization 1), irregular curves with zero and infinite slopes (Realization 2) and normal distributions (Realization 3). The parameter p-box has a certain distribution in the restricted region, but the distribution parameters are unknown. Both of them are introduced clearly in [29]. The type of p-box discussed in this article is free p-box, and it is the generalization of parametric p-box and called p-box in the rest of this article. In particular, the p-box variables degenerate into random variables, if $\underline{F}_{\mathbf{P}}(\mathbf{p}) = \bar{F}_{\mathbf{P}}(\mathbf{p})$.

According to the reliability theory of system structure, when the system contains both random variable \mathbf{X} and p-box variable \mathbf{P} , the expression of system failure probability is defined as

$$P(G(\mathbf{X}, \mathbf{P}) \leq 0) = \iint_{G(\mathbf{X}, \mathbf{P}) \leq 0} f_{\mathbf{X}, \mathbf{P}}(\mathbf{x}, \mathbf{p}) d\mathbf{x}d\mathbf{p}, \quad (2)$$

where $G(\mathbf{X}, \mathbf{P})$ and $f_{\mathbf{X}, \mathbf{P}}(\mathbf{x}, \mathbf{p})$ respectively denote the limit state

function and the joint probability density function (PDF). The failure probability is an interval value, which can be expressed as

$$\begin{bmatrix} \overline{P_f} \\ \underline{P_f} \end{bmatrix} = \begin{bmatrix} \sup \\ \inf \end{bmatrix}_{x \in D_x, p \in D_p} \iint_{G(X,P) \leq 0} f_{X,P}(x, p) dx dp, \quad (3)$$

where D_x and D_p are the value space of \mathbf{X} and \mathbf{P} respectively, \sup and \inf represent the minimum upper bound and maximum lower bound respectively.

2.2. Interval Monte Carlo simulation

In Monte Carlo simulation, the probability of failure is approximated as

$$P_f = \frac{1}{n_{mc}} \sum_{j=1}^{n_{mc}} I[G(X^{(j)}) \leq 0], \quad (4)$$

where n_{mc} is the total number of simulations conducted, $X^{(j)}$ represents the j th randomly simulated vector of basic variables, and $j=1, 2, \dots, n_{mc}$. $I[\cdot]$ is the indicator function, having the value 1 if $[\cdot]$ is 'true', and the value 0 if $[\cdot]$ is 'false'.

For calculating the lower and upper bounds of the failure probability, the Monte Carlo simulation is extended to the case where the variables are p-box variables, the new process is called Interval Monte Carlo simulation (IMCS)[40].

For limit state function $G(\mathbf{X}, \mathbf{P})$, where \mathbf{X} represents random variable, \mathbf{P} represents n -dimensional p-box variables, and the corresponding CDFs of each p-box variable is expressed as $F_{P_i}(p) \in [F_{P_i}^-(p), \overline{F}_{P_i}(p)]$, $i=1,2,\dots,n$, the main process of interval Monte Carlo method is as follows:

Step 1: According to the inverse transform method and the CDF of the random variable \mathbf{X} , generate random sample $X^{(j)}$:

$$X^{(j)} = F_X^{-1}(r^{(j)}), \quad j = 1, 2, \dots, n_{mc}, \quad (5)$$

where $r^{(j)}$ is the j th sample by [0,1] uniform distribution;

Step 2: Generate p-box sample $\mathbf{P}^{(j)}$. By the inverse transform method[27], the interval $[\underline{P}_i^{(j)}, \overline{P}_i^{(j)}]$ of i th p-box sample $P_i^{(j)}$ can be gained by

$$\begin{cases} \overline{P}_i^{(j)} = F_{P_i}^{-1}(c_i^{(j)}) \\ \underline{P}_i^{(j)} = \overline{F}_{P_i}^{-1}(c_i^{(j)}) \end{cases}, \quad (6)$$

where $c^{(j)} = [c_1^{(j)} \dots c_n^{(j)}]$ is generated by [0,1] uniform distribution. The value space formed by Eq. (6) is

$$D_{c^{(j)}} = [\underline{P}_1^{(1)}, \overline{P}_1^{(1)}] \times \dots \times [\underline{P}_n^{(j)}, \overline{P}_n^{(j)}].$$

Step 3: To calculate the upper and lower limits of the failure probability, the maximum and minimum values of the limit state function on this interval should be obtained by

$$\begin{cases} \overline{G}^{(j)} = \max_{P \in D_{c^{(j)}}} G(X^{(j)}, P^{(j)}) \\ \underline{G}^{(j)} = \min_{P \in D_{c^{(j)}}} G(X^{(j)}, P^{(j)}) \end{cases}, \quad (7)$$

Step 4: Repeat Step 1 to 3 until the maximum number n_{mc} of samples is met. The upper bound on the probability of failure is determined by $\underline{G}^{(j)}$, while the lower bound is determined by $\overline{G}^{(j)}$. According to the Monte Carlo simulation, the upper and lower limits of failure probability can be expressed as

$$\underline{P_f} = \frac{1}{n_{mc}} \sum_{j=1}^{n_{mc}} I(\overline{G}^{(j)} \leq 0) \leq P_f \leq \overline{P_f} = \frac{1}{n_{mc}} \sum_{j=1}^{n_{mc}} I(\underline{G}^{(j)} \leq 0), \quad (8)$$

MCS can effectively calculate the failure probability boundary of systems with p-box variables, which has become the cornerstone of the development of random sampling methods. However, when dealing with complex system functions, IMCS's efficiency is compromised by the requirement for numerous function calls and complex optimization calculations. Moreover, when the limit state function is expressed implicitly, the process of obtaining the maximum and minimum values necessitates intricate optimization calculations using the interval finite element method. As the number of sampling instances increases, the time required by IMCS grows exponentially. Additionally, the accuracy of IMCS's boundary estimation depends on the precision of extreme point calculations. Considering that it is unreasonable to regard the statistical result of extreme points on each interval as the final outcome, the accuracy of IMCS is compromised in scenarios involving complex non-monotonic problems where simultaneous attainment of extreme points across intervals is unattainable.

It is evident from the discussion on p-box theory in Section 2.1 that p-box variables are not entirely unconstrained within their upper and lower limits. Instead, they possess an unknown yet distinct distribution that adheres to the distribution principles governing general random variables. When represented on the cumulative distribution function graph, the curve does not exhibit a downward trajectory. This implies that the slope of the curve at any given point is non-negative.

The sampling process of IMCS is described by taking two

adjacent samples as an example. The steps are as follows:

Step 1: Suppose there is a two-dimensional p-box variable $P=[P_1, P_2]$, according to the uniform distribution of $[0, 1]$, two samples are successively generated. Suppose that the two samples ($c^{(1)}=[c_1^{(1)}, c_2^{(1)}]$) and $c^{(2)}=[c_1^{(2)}, c_2^{(2)}]$) are close enough.

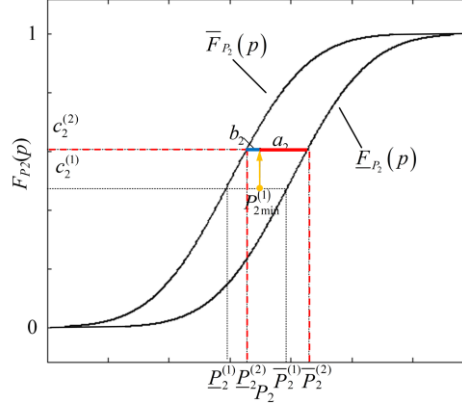
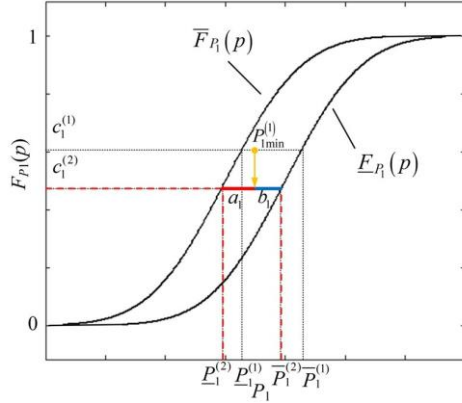


Fig. 2. Diagram of the adjacent sampling process.

Step 3: As shown in Fig. 2, the value intervals of samples $P_1^{(2)}$ and $P_2^{(2)}$ obtained in the second sampling $c^{(2)}$ are divided into two regions by $P_{1min}^{(1)}$ and $P_{2min}^{(1)}$, respectively, called a_1, b_1 and a_2, b_2 . When the function is complex and P_1 and P_2 are not completely monotonic, minimum point $P_{min}^{(2)}=[P_{1min}^{(2)}, P_{2min}^{(2)}]$ corresponding to $c^{(2)}$ can occur anywhere along the entire range.

Step 4: If $P_{1min}^{(2)}$ and $P_{2min}^{(2)}$ are located in a_1 and a_2 respectively, the CDFs' images don't show a downward trend, it also means that the two minimum points can be obtained from the same distribution. When one or both of $P_{1min}^{(2)}$ and $P_{2min}^{(2)}$ are located in b_1 and b_2 , the CDFs' images tend to go down, so these two extreme points cannot be in the same distribution.

The process means that the true value intervals of $P_1^{(2)}$ and $P_2^{(2)}$ are a_1 and a_2 , but not $[P_1^{(2)}, P_1^{(2)}]$ and $[P_2^{(2)}, P_2^{(2)}]$. Therefore, when the minimum of the limit state function solved by IMCS optimization is less than 0, the real minimum on the real value interval may be greater than 0. Because IMCS cannot identify the real value interval well, the upper bound of failure probability is overestimated. The process of solving function maximum by IMCS optimization is similar, leading to a smaller lower bound of failure probability.

For one-dimensional p-box variables or completely monotone cases, IMCS can accurately calculate the upper and lower limits of the failure probability, avoiding the previously mentioned phenomenon. However, when confronted with two-dimensional non-monotonic p-box variables or higher-

Step 2: The maximum and minimum values ($\bar{G}^{(1)}$ and $\underline{G}^{(1)}$) of the limit function corresponding to the first sampling are obtained according to IMCS. The sample points on the p-box variable interval corresponding to the extreme value are $P_{max}^{(1)}$ and $P_{min}^{(1)}$ respectively, $P_{min}^{(1)}=[P_{1min}^{(1)}, P_{2min}^{(1)}]$ is shown in Fig. 2

dimensional scenarios, IMCS unavoidably encounters the challenges discussed in this section. These challenges highlight areas where further improvements are necessary for IMCS.

3. New Method Based on Weight Coefficients and Important Sampling

To enhance computational efficiency and address the challenges mentioned in the preceding section, a novel reliability analysis method for systems with p-box variables is proposed. The new approach constructs an optimization model of failure probability based on failure samples and weights, enabling the calculation of upper and lower bounds for failure probability. Firstly, the p-box variables are discretized into a series of sub-intervals, and each interval is assigned a different weight index. The failure probability is given by the ratio between the sum of the weights corresponding to the failure samples and the sum of the total samples. The main steps are as follows:

Step 1: Determine auxiliary input variables for each p-box variable and compute design points using the limit state functions. Then the initial failure probability is approximated by importance sampling and the number of failure sample points is obtained.

Step 2: Employ the auxiliary input variables to discretize the p-box variables and establish corresponding weight coefficients for each interval.

Step 3: Update the number of samples based on the

maximum interval weight, coefficient of variation, and initial number of failure samples to mitigate the adverse effects of excessive weight coefficients on the results. Obtain the failure samples used to construct the failure probability equation.

Step 4: Establish the optimization function for failure probability and solve for the upper and lower bounds of failure probability through optimization techniques.

By implementing these steps, the proposed method offers a more efficient approach to reliability analysis, effectively addressing the limitations of the conventional IMCS approach. The flowchart is shown in Fig. 3. The calculation of interval weight and the construction of the failure probability equation are the basis of the whole algorithm and the key ensuring the accuracy of the results. This paper divides the entire process into two modules for presentation.

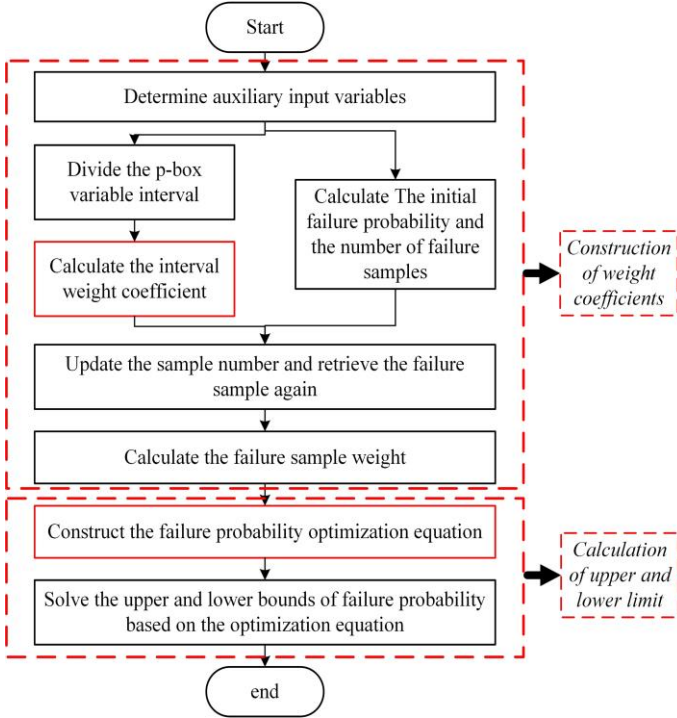


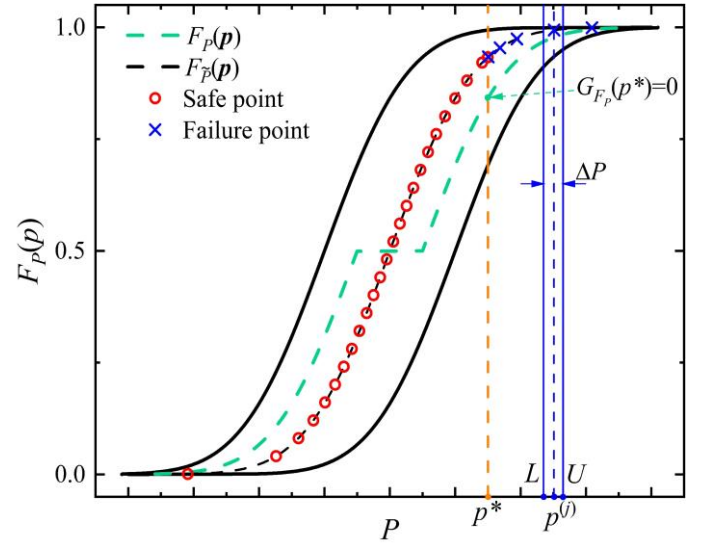
Fig. 3. Flowchart of the proposed method.

1.1. Construction of weight coefficients

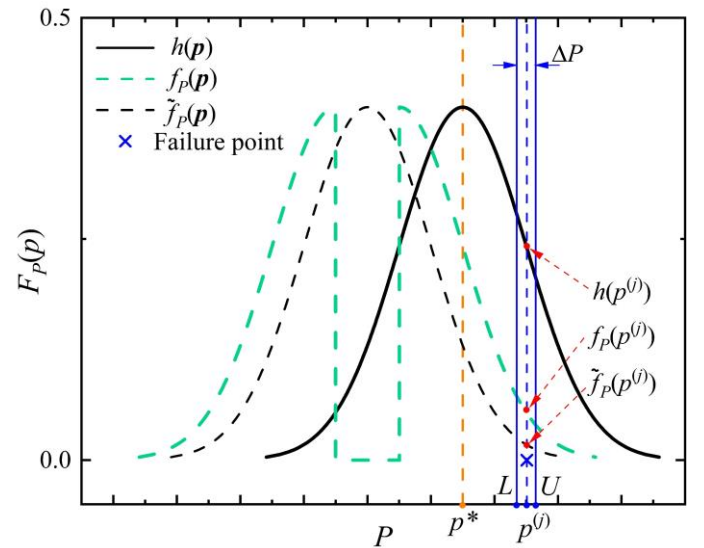
In the following analysis, we focus on the incorporation of P-box variables in reliability analysis, as the inclusion of random variables can be readily implemented. In other words, the system is considered to contain only n -dimensional independent p-box variable \mathbf{P} , and the limit state function is $\mathbf{G}(\mathbf{P})$. Firstly, the auxiliary input variable[29] is introduced to approximate the p-box variable, whose expression is

$$F_{\tilde{\mathbf{P}}}(\mathbf{p}) = \frac{1}{2}(F_{\mathbf{P}}(\mathbf{p}) + \bar{F}_{\mathbf{P}}(\mathbf{p})). \quad (9)$$

The joint probability density function (PDF) of auxiliary input variables is denoted as $\tilde{f}_{\mathbf{P}}(\mathbf{p})$. The auxiliary input distribution is selected to encompass the region where the majority of the p-box variables are located. This distribution aims to capture the essential characteristics of the p-box variables to the fullest extent possible. Additionally, it serves as the basis for importance sampling of the p-box variables and serves as a reference for dividing intervals.



(a) MCS sampling of p-box variable failure samples



(b) Failure sample weight mapping based on PDFs

Fig. 4. Failure sample weight construction diagram.

As shown in Fig. 4(a), the real CDF of the p-box is $F_{\mathbf{P}}(\mathbf{p})$, and its PDF is $f_{\mathbf{P}}(\mathbf{p})$. When $G(p^*)=0$, $p=p^*$ is called the critical point. According to Eq. (4), MCS calculates the failure probability by collecting failure samples. In order to obtain sufficient failure samples to construct the optimization equation

and obtain a more accurate interval distribution of failure samples, the important sampling method is used to sample the auxiliary input function. This paper uses the same distribution type as $\tilde{f}_P(\mathbf{p})$ to construct the important sampling function $h(\mathbf{p})$. For example, if $\tilde{f}_P(\mathbf{p}) \sim N(p, \sigma)$, $h(\mathbf{p}) \sim N(p^*, \sigma)$. The p-box variables are sampled for the first time according to $h(\mathbf{p})$, and the number of samples is n_{mco} . Eq. (4) is rewritten as

$$P_f = \frac{1}{n_{mco}} \sum_{j=1}^{n_{mco}} I[G(\mathbf{p}^{(j)}) \leq 0] \cdot \frac{\tilde{f}_P(\mathbf{p}^{(j)})}{h(\mathbf{p}^{(j)})}, \quad (10)$$

where $j=1, \dots, n_{mco}$. According to Fig. 4(b), the weight of the sample $\mathbf{p}^{(j)}$ composed of important samples can be obtained and written as

$$W_{IS}^{(j)} = \frac{\tilde{f}_P(\mathbf{p}^{(j)})}{h(\mathbf{p}^{(j)})}. \quad (11)$$

Inspired by important sampling, the failure sample on the auxiliary input variable can be projected into the p-box space by using the real p-box variable PDF, and the weight of the failure sample is

$$W_{IN}^{(j)} = \frac{f_P(\mathbf{p}^{(j)})}{\tilde{f}_P(\mathbf{p}^{(j)})}. \quad (12)$$

As shown in Fig. 1, $f_P(\mathbf{p})$ is unknown and could equal infinity. Therefore, the weight on the neighborhood of the failure sample is used to approximate the weight of this point. The nodes in the neighborhood interval are denoted as $[L, U]$, and Eq. (12) is rewritten as

$$W_{IN}^{(j)} = \frac{\int_L^U f_P(\mathbf{p}) d\mathbf{p}}{\int_L^U \tilde{f}_P(\mathbf{p}) d\mathbf{p}} = \frac{Pr}{\int_L^U \tilde{f}_P(\mathbf{p}) d\mathbf{p}} \quad (13)$$

When ΔP is small enough, the physical meaning of Pr in Fig. 4(a) is related to the slope $\theta^{(j)}$ of the p-box's CDF over the neighborhood, which is approximately calculated as

$$Pr = F_P(U) - F_P(L) = \theta^{(j)}(U - L). \quad (14)$$

According to Eq.(11) and (13), each failure sample is assigned an important sample weight and an interval weight respectively. After the weights of all failure samples are calculated, the failure probability of this group of samples projected onto the p-box space can be obtained by the simultaneous Eq. (10)~(13) as

$$P_f = \frac{1}{n_{mco}} \sum_{j=1}^{n_{mco}} I[G(\mathbf{p}^{(j)}) \leq 0] \cdot \frac{\tilde{f}_P(\mathbf{p}^{(j)})}{h(\mathbf{p}^{(j)})} \cdot \frac{Pr}{\int_L^U \tilde{f}_P(\mathbf{p}) d\mathbf{p}} \quad (15)$$

Since $F_P(\mathbf{p})$ and $f_P(\mathbf{p})$ are unknown on the p-box space, Eq. (15) cannot be solved directly. By introducing the interval discretization method, the interval weights $W_{IN}^{(j)}$ of samples $\mathbf{p}^{(j)}$ are reconstructed. The specific steps are as follows:

Step 1: $j=1, i=1$. j denotes the j th sampling, and i denotes the i th p-box variable;

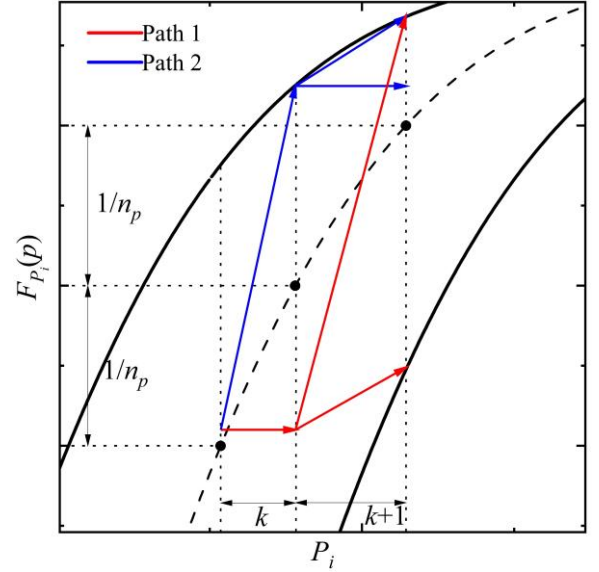


Fig. 5. Construction diagram of interval weight constraints.

Step 2: Interval partition is performed for the i th p-box variable. Since the interval length of each variable is different, uniform discretization is carried out on the vertical axis of $F_{P_i}(\mathbf{p})$, and the discretization number is n_p . As shown in Fig. 5, the k th and $k+1$ th interval nodes of i th p-box are $[L_i^{(k)}, U_i^{(k)}]$ and $[L_i^{(k+1)}, U_i^{(k+1)}]$, respectively. According to Eq. (13), $\int_{L_i^{(k)}}^{U_i^{(k)}} \tilde{f}_P(\mathbf{p}) d\mathbf{p} = \int_{L_i^{(k+1)}}^{U_i^{(k+1)}} \tilde{f}_P(\mathbf{p}) d\mathbf{p} = \frac{1}{n_p}$, and the integrals of $f_{P_i}(\mathbf{p})$ over the two intervals are denoted as $Pr_i^{(k)}$ and $Pr_i^{(k+1)}$, $k=1, \dots, n_p-1$;

Step 3: Put constraints on $Pr_i^{(k)}$. Due to the i th p-box has bounds $\underline{F}_{P_i}(\mathbf{p})$ and $\overline{F}_{P_i}(\mathbf{p})$, $Pr_i^{(k)}$ can be expressed as $Pr_i^{(k)} \in [Pr_{i_{min}}^{(k)}, Pr_{i_{max}}^{(k)}]$. According to the discussion in Section 2.2 that $F_P(\mathbf{p})$ should not have a downward trend and Eq. (14), $Pr_{i_{min}}^{(k)} = 0$ and $Pr_{i_{max}}^{(k)} = \overline{F}_{P_i}(U_i^{(k)}) - \underline{F}_{P_i}(L_i^{(k)})$. When $F_{P_i}(\mathbf{p})$ enters the $k+1$ th interval along path 1, $Pr_i^{(k+1)} \in [\underline{F}_{P_i}(U_i^{(k+1)}) - \overline{F}_{P_i}(L_i^{(k+1)}), \overline{F}_{P_i}(U_i^{(k+1)}) - \underline{F}_{P_i}(L_i^{(k+1)})]$. When $F_{P_i}(\mathbf{p})$ enters the $k+1$ th interval along path 2, $Pr_i^{(k+1)} \in [0, \overline{F}_{P_i}(U_i^{(k+1)}) - \underline{F}_{P_i}(L_i^{(k+1)})]$. After extending the slope trend of the two intervals to all intervals, the constraint equation of the value of any interval $Pr_i^{(k)}$ is

$$\begin{cases} Pr_{i_{min}}^{(k)} \max[\underline{F}_{P_i}(U_i^{(k)}) - \overline{F}_{P_i}(L_i^{(k)}), 0] \\ Pr_{i_{max}}^{(k)} \overline{F}_{P_i}(U_i^{(k)}) - \underline{F}_{P_i}(L_i^{(k)}) \end{cases} \quad (16)$$

where $\bar{F}_{P_i}(U_i^{(n_p)}) = \underline{F}_{P_i}(U_i^{(n_p)}) = 1, \bar{F}_{P_i}(L_i^{(1)}) = \underline{F}_{P_i}(L_i^{(1)}) = 0$ and $k=1, \dots, n_p$;

Step 4: Construct the sample $\mathbf{p}^{(j)}$'s interval weights. Then $i=i+1$, when $i=n$, all p-box variables are discretized. The corresponding interval number of n -dimensional samples $\mathbf{p}^{(j)}$ is $k^{(j)}=[k_1^{(j)}, \dots, k_n^{(j)}]$, the weight due to the discrete interval is denoted as $W_{IN}^{(j)}$, represents the ratio of the two probabilities involved in Step 2. According to Eq. (13), the sample interval weight is rewritten as

$$W_{IN}^{(j)} = (n_p)^n \prod_{i=1}^n \Pr_i^{(k_i^{(j)})}. \quad (17)$$

Step 5: $j=j+1$, when $j=n_{mc0}$, the sampling ends.

To sum up, the sample weight index consists of $W_{IS}^{(j)}$ and $W_{IN}^{(j)}$.

$$W^{(j)} = W_{IS}^{(j)} W_{IN}^{(j)} = \frac{\bar{f}_P(\mathbf{p}^{(j)})}{h(\mathbf{p}^{(j)})} (n_p)^n \prod_{i=1}^n \Pr_i^{(k_i^{(j)})}, \quad (18)$$

where $\Pr_i^{(k_i^{(j)})}$ is a particular combination of $\Pr_i^{(k)}$. When $\Pr_i^{(k)}$ is treated as a group of unknown parameters, the weight can be used to convert the failure probability into a function of $\Pr_i^{(k)}$, and the dimension is $n \times n_p$.

3.1. Calculation of upper and lower limit of failure probability

In order to prevent the increase of interval weight index $W_{IN}^{(j)}$, caused by too large $\Pr_i^{(k)}$, thus affecting the accuracy of the solution, the proposed method sets two independent sampling. After the first sampling, the initial number of failed samples (n_{Fail}) and the coefficient of variation of failure probability ($Cov(P_f)$) are calculated according to the results of important sampling. After calculating $\Pr_i^{(k)}$, the sample number is updated to be

$$n_{mc} = \max\left[\frac{n_{mc0} \cdot \max(n_p \Pr_i^{(k)})}{n_{Fail} \cdot Cov(P_f)^2}, 100 \times n_p\right]. \quad (19)$$

This means making it as large as possible without compromising accuracy. The purpose is to reduce the influence of excessive weight coefficient on the results and ensure the minimum sampling number. According to Eq. (18), Eq. (15) can be rewritten as

$$\begin{aligned} P_f &= \frac{1}{n_{mc}} \sum_{j=1}^{n_{mc}} I[G(\mathbf{p}^{(j)}) \leq 0] \cdot W^{(j)} = \frac{1}{n_{mc}} \sum_{j=1}^{n_{mc}} I[G(\mathbf{p}^{(j)}) \\ &\leq 0] \cdot \frac{\bar{f}_P(\mathbf{p}^{(j)})}{h(\mathbf{p}^{(j)})} (n_p)^n \prod_{i=1}^n \Pr_i^{(k_i^{(j)})}. \end{aligned} \quad (20)$$

Eq. (20) is the equation for the variable $\Pr_i^{(k)}$. $\Pr_i^{(k)}$ has a series of linear constraints, so that the problem can be transformed into a multivariable linear constrained optimization problem. Combined with Eq. (16), its constraints D_{Pr} are constructed as follows

$$\begin{cases} \sum_{k=1}^K \Pr_i^{(k)} \in [\underline{F}_{P_i}(U_i^{(k)}), \bar{F}_{P_i}(U_i^{(k)})], K = 2, 3, \dots, n_p - 1 \\ \Pr_i^{(k)} \in [\Pr_{imin}^{(k)}, \Pr_{imax}^{(k)}] \mid \sum_{k=1}^{n_p} \Pr_i^{(k)} = 1 \end{cases} \quad (21)$$

where $i=1, \dots, n$.

Through the optimization solution of Eq. (20) under constraints D_{Pr} , upper and lower bounds of failure probability can be obtained. The expression of upper and lower bounds is

$$\begin{cases} \bar{P}_f = \max_{\Pr_i^{(k)} \in D_{Pr}} P_f \\ \underline{P}_f = \min_{\Pr_i^{(k)} \in D_{Pr}} P_f \end{cases}. \quad (22)$$

When Eq. (22) is used to solve the upper and lower bounds of the failure probability, the solutions corresponding to the upper and lower bounds satisfying the convergence condition of the optimization algorithm are the optimal solutions \bar{P}_f^* and \underline{P}_f^* .

Using Eq. (14) and (17), the weights (\bar{W}_{IN}^* and \underline{W}_{IN}^*) of the optimal interval and the slopes ($\bar{\theta}^*$ and $\underline{\theta}^*$) of the curve on the corresponding interval can be calculated. Given the interval nodes, the boundary curves corresponding to the upper and lower bounds of the failure probability can be obtained by linear fitting. Moreover, because the solutions \bar{P}_f^* and \underline{P}_f^* satisfies constraint Eq. (16), the rationality of the curve trend can be guaranteed, and CDFs' trend as shown in Section 2.2 will not appear.

From the above discussion, after comparing Eq. (22) and Eq. (7), it is found that the new method uses MCS to obtain limit state function $\mathbf{G}(\mathbf{P})$'s failure samples at one time to build optimization equations, the process of solving the failure model does not need $\mathbf{G}(\mathbf{P})$. However, IMCS needs $\mathbf{G}(\mathbf{P})$ to calculate the extreme value of $\mathbf{G}(\mathbf{P})$ in each sampling. In other words, the optimization model complexity adopted by the new method is independent of $\mathbf{G}(\mathbf{P})$'s complexity, but is only affected by the dimensions of the model itself. The complexity of the optimization model used in IMCS is proportional to the complexity of $\mathbf{G}(\mathbf{P})$.

The proposed p-box variable analysis method has the following advantages: (1) The upper and lower limits of the failure probability can be obtained by only two optimization

searches with linear constraints. (2) It ensures the inherent characteristics of p-box variable distribution, and avoids the problem of obtaining a larger failure probability interval when IMCS deals with complex problems; (3) The approximate cumulative distribution function of the p-box variable can be obtained at the same time as the failure probability boundary; (4) The performance function does not need to be called again during the calculation.

4. Case Study and Discussion

Six different cases are selected to verify that the proposed method has higher efficiency and accuracy than IMCS and the method proposed by Xie et al[36](Xie's for short). It should be noted that the six cases represent different models in typical computational examples and actual projects, and they have performance functions and variable structures of different complexity levels. The application of the proposed method in these cases also indicates its universality and can be extended.

4.1. Case Study 1: Single p-box variable problem

This case is used to verify the correctness of the proposed method. x is a p-box variable, and its mean value is bounded in the intervals $[1.4, 1.6]$ and its standard deviation is 1. The performance function is defined as

$$G(x) = 2 - \frac{x^2+4}{20} + \sin\left(\frac{5x}{2}\right). \quad (23)$$

The results are shown in

Table 1, which provides the number of partition intervals n_p , the lower and upper bounds of failure probability (\underline{P}_f and \overline{P}_f), the relative errors and the Number of Function calls (NFC).

Table 1. Results of Case 1.

Method	n_p	\underline{P}_f (Error %)	\overline{P}_f (Error %)	NFc
IMCS	-	0.0015	0.0039	10^5
Xie's	50	0.0016(6.66)	0.0042(7.67)	200
The proposed method	10	0.0018(20)	0.0035(10.25)	4
	20	0.0016(6.66)	0.0038(2.56)	
	30	0.00148(1.3)	0.00386(1.0)	
	40	0.00148(1.3)	0.00388(0.3)	

The IMCS, Xie's and proposed method are used for calculation, and the results are shown in

Table 1. The upper and lower bounds of failure probability calculated by IMCS are 0.0015 and 0.0039, respectively. When $n_p=50$, the upper and lower bounds of failure probabilities calculated by Xie's are 0.0016 and 0.0042, and the relative errors are 6.66% and 7.67% respectively. When the proposed method is used, the results calculated at $n_p=40$ are **0.00148** and **0.00388** respectively, with relative errors of **1.3%** and **0.3%**. The extreme value points obtained by IMCS and the variable boundaries fitted by Xie's and the proposed method are plotted, as shown in Fig. 6(a). It can be seen that there are obvious differences between the fitting curves and the distributions of extreme points, so the interval distribution of failure samples in the calculation process of the proposed method is further analyzed. When $n_p=40$, the failure samples are concentrated in the interval 34-40. The failure point obtained by IMCS, and the variable boundary fitted by Xie's and the proposed method in the interval 34-40 are plotted in Fig. 6(b). It can be found that the fitting curve of the proposed method is almost consistent with the distribution of IMCS failure sample points, while the fitting curve of Xie's is significantly different. It shows that the proposed method can well approximate the variable distribution in the failure sensitive region and obtain the accurate failure probability boundary

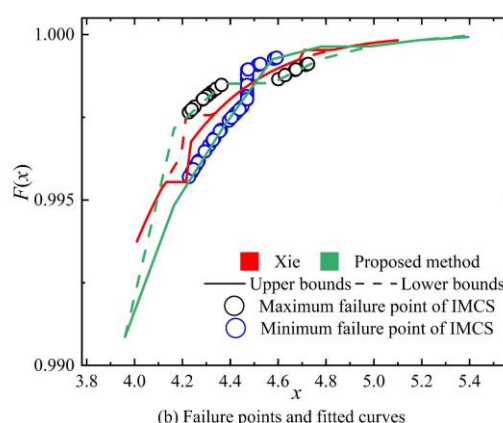
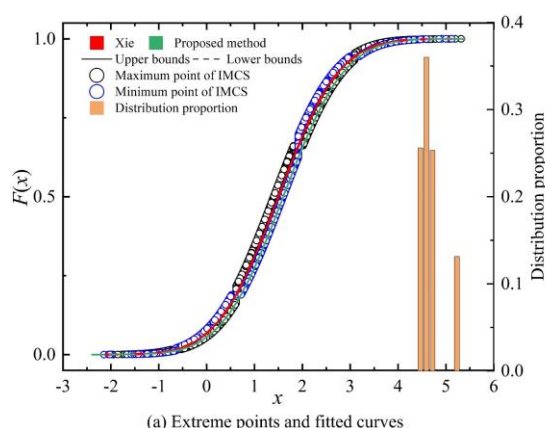


Fig. 6. Point distribution and fitting curves of Case 1.

The failure probability boundary curves and corresponding relative errors of the latter two methods under different discrete points are calculated and plotted, as shown in Fig. 7. It can be seen that with the increase of n_p , the lower and upper bounds of the failure probabilities yielded by the two methods gradually approach the reference solution, while the relative errors decrease. When $n_p < 100$, the relative error of the proposed

method is always below 20%, while the maximum error of Xie's can reach 70%. According to Fig, when the relative errors of both limits are lower than 5%, the n_p required by Xie's is 250, while the n_p required by the proposed method is 25, which is much lower than the former. It means that the proposed method can converge to the exact boundary faster than Xie's as n_p increases.

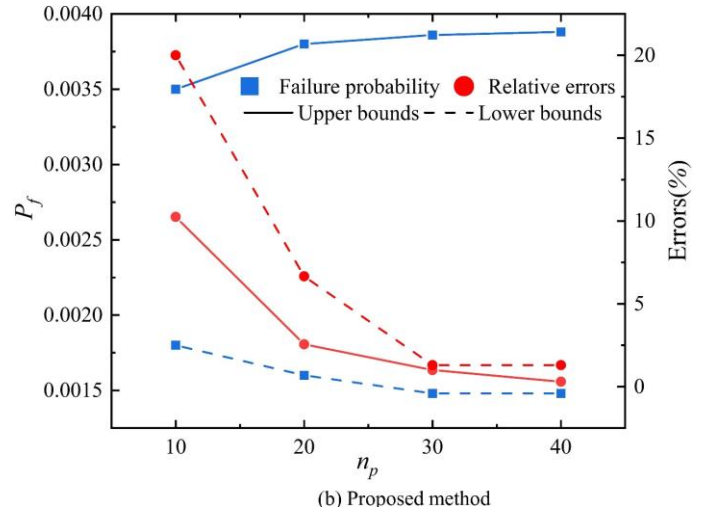
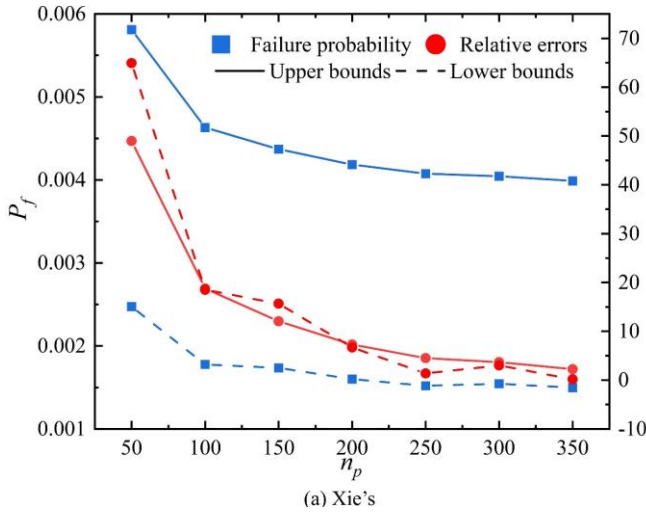


Fig. 7. Failure probability boundaries and relative errors of Case 1,

Count the number of functions calls (NFC) for each method when considering computational efficiency. IMCS uses the original function to optimize the solution in each loop, so the NFC is the number of sampling 10^5 . The NFC of Xie's is $2 \times 2 \times 50$, concluding two optimizations, two iterations in each optimization and calculating conditional failure probabilities 50 times in each iteration. The total NFC of the proposed method is 4, of which the number of calls of the original function is 2, and the number of calls of the optimization function is 2. It is far lower than the first two methods. In the proposed method, the dimensionality of the optimization function keeps growing linearly with the increase of n_p . It means the increase in computation caused by n_p is controllable, and the above results show that the proposed method has higher computational efficiency than the previous two methods.

$$G(x, y) = 2 - \frac{(x-1)(y^2+4)}{20} + \sin\left(\frac{5y}{2}\right), \quad (24)$$

where x is a normal variable and y is a p-box variable, listed in Table 2.

Table 2. Distribution of random variables for case 2.

Variables	Distribution type	Mean	Standard deviation
x	Normal	2.5	1
y	Normal	[1.4,1.6]	1

The three methods are used to calculate and plot the failure probability curves, and the results are shown in Table 3 and Fig. 8, with three significant figures reserved. It can be seen that with the increase of n_p , the upper and lower bounds of the failure probabilities of the two methods gradually converge. Compared with Xie's, the proposed method has faster convergence and smaller errors. When $n_p=50$, the relative errors of the upper and lower bounds of the proposed method are **2.98%** and **2.22%**, respectively, which are lower than 9.29% and 4.56% of Xie's. When $n_p=1000$, the lower and upper bounds proposed by Xie's converge to 0.204 and 0.429, which are slightly different from 0.0202 and 0.0436 calculated by IMCS. After calculating the relative error between the proposed method and the former, it is

found that the Errors (Xie 1000) are all lower than the Errors (IMCS). Both the lower bounds' errors (Xie 1000) and upper bounds' errors (Xie 1000) are lower than 1%. It shows that the results of the proposed method are closer to those of Xie's. In

order to explain this phenomenon, the IMCS extreme points' distributions, the fitting variable boundaries of the other two methods, and the failure samples' distributions of the proposed method are plotted.

Table 3. The result of case 2.

Method	n_p	\underline{P}_f	Lower Error (IMCS)	Lower Error (Xie 1000)	\overline{P}_f	Upper Error (IMCS)	Upper Error (Xie 1000)	NFc
IMCS	-	0.0202	-	-	0.0436	-	-	10^5
	50	0.0221	9.29016	-	0.0456	4.56178	-	200
	500	0.0204	1.16273	-	0.0430	1.31717	-	2000
Xie's	1000	0.0204	0.75348	-	0.0429	1.64152	-	4000
	10	0.0244	20.75	19.56	0.0377	13.56	12.1	
	20	0.0226	11.70	10.6	0.0401	8.06	6.55	
The proposed method	30	0.0213	5.30	4.25	0.0414	4.96	3.41	
	40	0.0209	3.44	2.43	0.0423	3.00	1.42	
	50	0.0208	2.98	1.97	0.0426	2.22	0.628	4
	60	0.0206	1.91	0.907	0.0427	2.09	0.488	
	70	0.0206	1.82	0.822	0.0428	1.91	0.313	
	80	0.0206	1.73	0.729	0.0428	1.91	0.311	
	90	0.0205	1.62	0.620	0.0430	1.33	0.281	
	100	0.0205	1.36	0.369	0.0430	1.31	0.299	

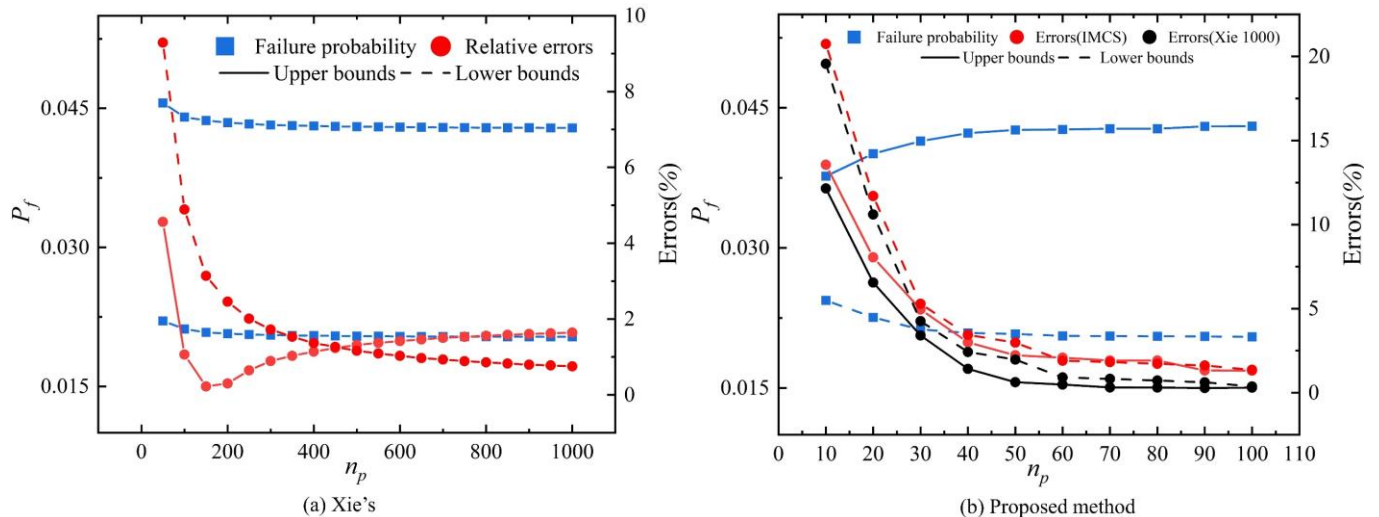


Fig. 8. Failure probability boundaries and relative errors of Case 2.

As shown in Fig. 9, it can be found that there are four distinct slope transition regions in both the extreme points' distributions and the fitting boundaries. In these four regions, the extreme points and failure points in the two positions on the right are scattered, as described in Section 2.2. After local amplification, it can be seen that the trend of curves fitted by the proposed method is consistent with that fitted by Xie's, and the unreasonable variables' distributions can be avoided in both cases. Most importantly, in Case 2, the fluctuation of extreme points mainly occurs in the failure sensitive regions, so it can be considered that the difference between the results of IMCS and

the other two methods is due to statistical errors caused by the distribution of extreme points. The above results show that the proposed method can approach the exact boundaries of p-box variables faster with small n_p , so as to obtain a tighter failure probability boundary.

In this case, the NFc of IMCS is 10^5 . When n_p is 50, 500, and 1000 respectively, the NFc of Xie's is 200, 2000, and 4000 in turn, increasing in proportion to n_p and the number of variables. The proposed method always calls the function 4 times, and the optimization function dimension increases with the increase of n_p and the number of variables. When $n_p=100$,

the dimension of the optimization function is 100.

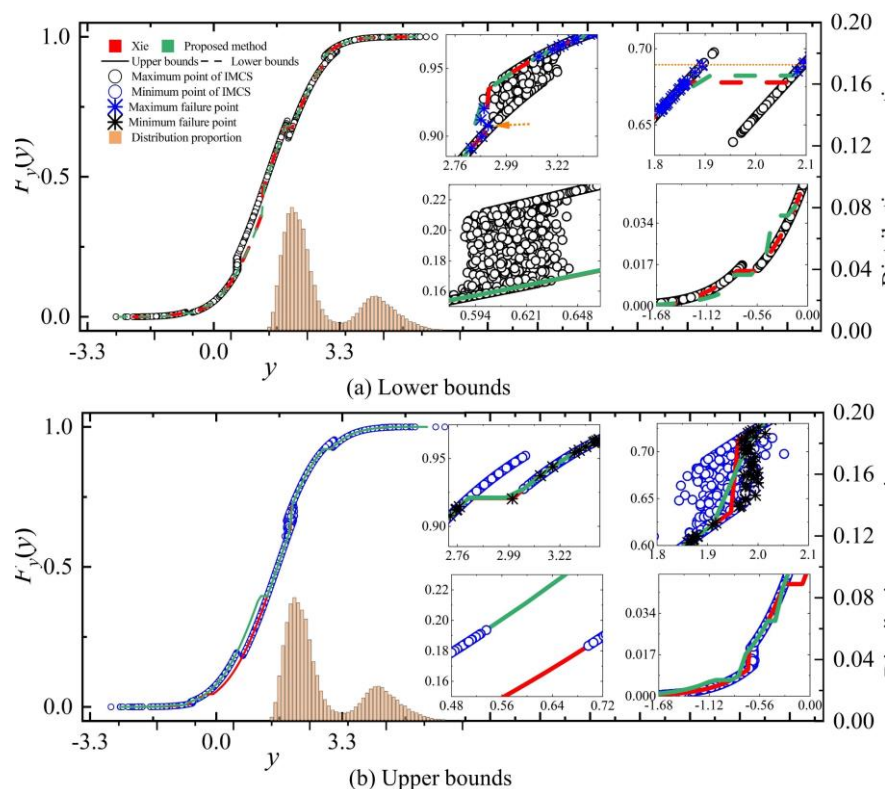


Fig. 9. Point distribution and fitting curves of Case 2.

4.3. Case Study 3: A mathematical problem

This Case is quoted from Xie's [36], and the performance function is

$$G(Y_1, Y_2) = Y_2 + 0.1 \times (Y_1 - 2)^2 + Y_1 - 3 \quad (25)$$

where Y_1 and Y_2 are all non-parameterized P-box variables. Their details are listed in Table 4.

Table 4. Distribution of p-box variables for case 3.

Variables	Distribution type	Mean	Standard deviation
Y_1	Normal	[1.76,1.84]	0.3
Y_2	Normal	[1.67,1.73]	0.25

In Xie's [36], IMCS and Xie's are used to calculate Case 3. The sample number of IMCS is 10^6 , and the failure probability boundary calculated by IMCS is [0.0619,0.1196]. When the discrete number is 200, the failure probability boundary calculated by Xie's is [0.0606,0.1171], and the relative errors are 2.03% and 2.08%, respectively. By comparing the proposed method with the two methods in Case 3, the results are shown in Table 5 and Fig. 10. As shown in Fig. 11 and Fig. 12, it can be seen that the failure extreme points, in this case, show a monotonous trend, so IMCS can obtain an accurate failure probability boundary. The weight fitting curve obtained by the

proposed method can fully reflect the trend and can be regarded as the boundary curve. As shown in Table 5 and Fig. 10, with the increase of n_p , the accuracy of the proposed method is gradually improved. When $n_p > 20$, the errors of the upper and lower failure probability calculated by the proposed method are less than 1%. Compared with the results of Case 2, it further shows that the difference between the two methods mainly comes from the difference between the extreme point and the weight fitting boundary curve. Compared with the upper and lower bound errors of Xie's, it can be seen that the proposed method can obtain more accurate results at a smaller discrete cost. Further comparing the Nfc required by different methods, the proposed method has higher computational efficiency.

Table 5. The result of case 3.

Method	n_p	\underline{P}_f (Error %)	\overline{P}_f (Error %)	Nfc
IMCS	-	0.0619	0.1198	2.09×10^7
Xie's	50	0.0606(2.03)	0.1897(1.07)	7826
	10	0.06384(3.13)	0.118(1.34)	
The proposed method	20	0.06212(0.36)	0.1186(0.84)	4
	30	0.06214(0.39)	0.1198(0.17)	
	40	0.062(0.16)	0.1202(0.50)	
	50	0.06163(0.47)	0.1202(0.50)	
	60	0.06167(0.37)	0.1201(0.42)	
	70	0.0616(0.49)	0.1201(0.42)	

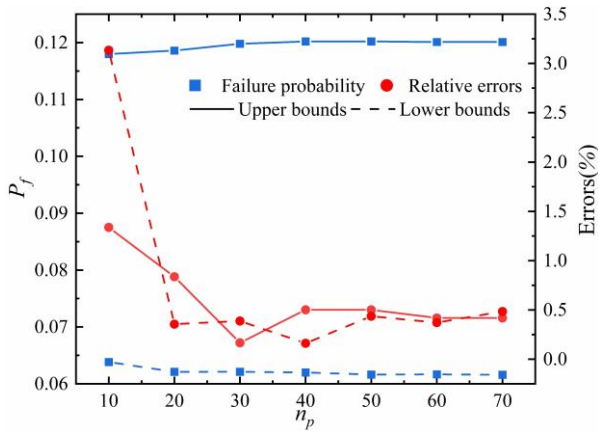


Fig. 10. Failure probability boundaries and relative errors of Case 3.

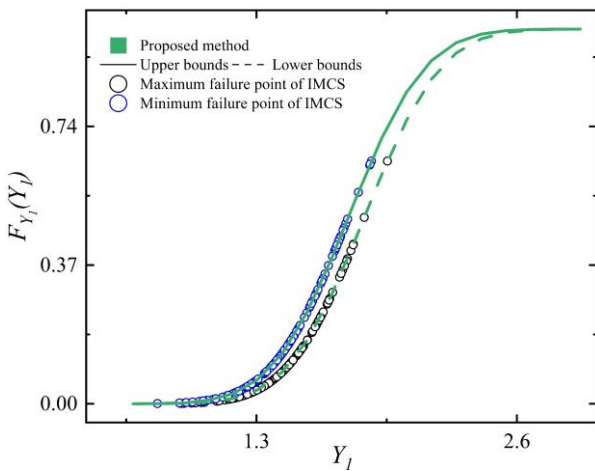


Fig. 11. Points distribution and fitting curves of Y_1 .

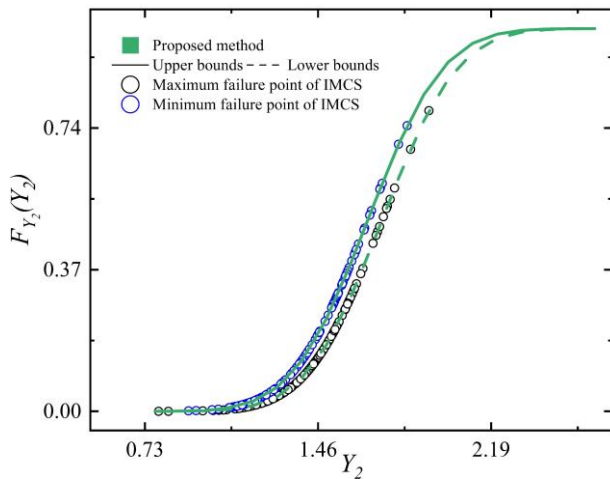


Fig. 12. Points distribution and fitting curves of Y_2 .

4.4. Case Study 4: A single-degree-of-freedom oscillator

Single degree of freedom oscillator is a common structure in engineering, and the oscillator problem is analyzed with multiple variables. It is a highly nonlinear undamped single-degree-of-freedom oscillator, including three random variables

and three p-box variables. Its schematic view is shown in Fig. 13, and the details about these variables are listed in Table 6.

The performance function is given as

$$G = 3r - \left| \frac{2F_1}{m\omega_0^2} \sin\left(\frac{\omega_0 t_1}{2}\right) \right|, \quad (26)$$

where r is the yield displacement of the springs, and ω_0 is calculated by

$$\omega_0 = \sqrt{\frac{c_1 + c_2}{m}}. \quad (27)$$

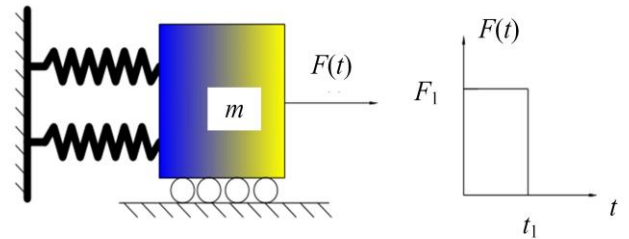


Fig. 13. Schematic diagram of a single-degree-of-freedom oscillator

Table 6. Distribution of variables for a single-degree-of-freedom oscillator

Variables	Distribution type	Mean	Standard deviation
c_1	Normal	1	0.1
c_2	Normal	0.1	0.01
m	Normal	1	0.05
r	Normal	[0.49,0.51]	0.05
F_1	Normal	[-0.2,0.2]	0.5
t_1	Normal	[0.95,1.05]	0.2

Three methods are used to calculate, and IMCS extremum points and fitting curves are plotted. As shown in Fig. 14-16, the extreme value points of IMCS show a reasonable distribution trend, which means that IMCS can obtain accurate calculation results. For r and t_1 , both the proposed method and Xie's can better approximate the distribution curve. But when according to F_1 , the slope of IMCS maximum points' distribution and minimum points' distribution appear to be non-existent and zero respectively in the interval $[-0.4,0]$. The slope variation interval of the curves fitted by the proposed method is $[-0.44, -0.088]$, which captures the change trend of the distribution curve well and achieves a better fitting effect in the whole interval. The slope variation positions of the fitting curves yielded by Xie's are the interval $[-0.6, -0.18]$ and $F_1=0.616$ respectively, which has a large deviation from the distribution curves. It shows that with the increase of variables and their complexity, the proposed

method can approach the variables' boundaries more accurately.

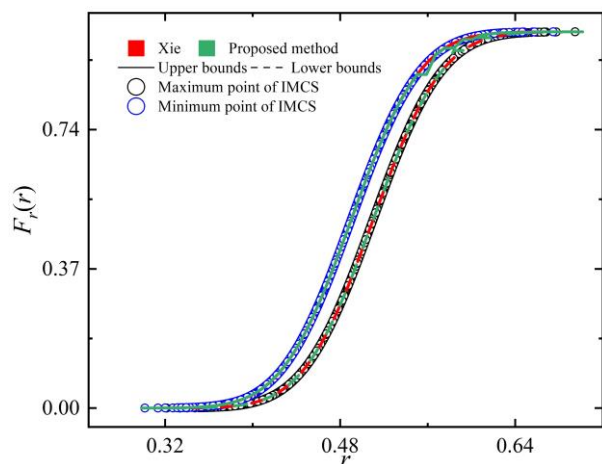


Fig. 14. Points distribution and fitting curves of r .

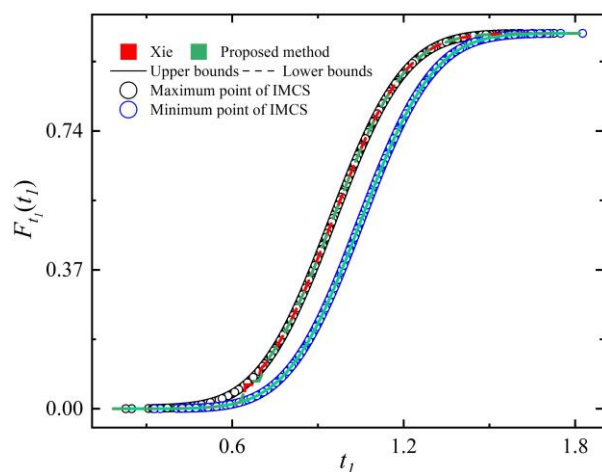


Fig. 15. Points distribution and fitting curves of F_1 .

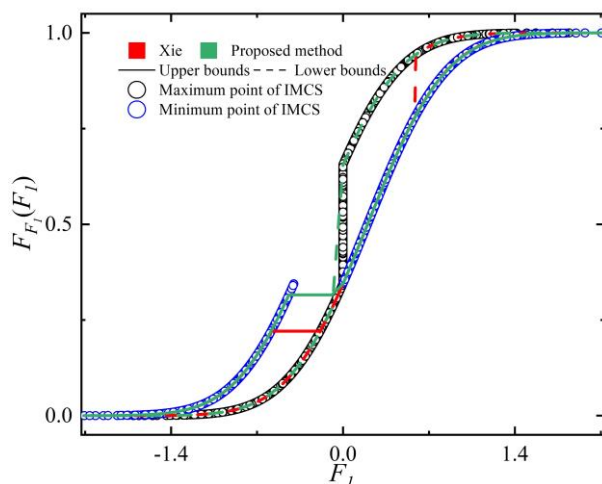


Fig. 16. Points distribution and fitting curves of t_1 .

As Table 7 listed, the upper and lower bounds of failure probability calculated by IMCS are 0.00065 and 0.0159. Calculate and plot the failure probability bounds and relative errors of the proposed method and Xie's at different n_p . As

shown in Fig. 17, with the increase of n_p , the results of the proposed method approach the IMCS results gradually, and the relative errors decrease continuously. When n_p exceeds 30, the results of the proposed method converge, and the relative errors of the upper and lower bounds are less than 5%. Although the lower bound of Xie's presents a decreasing trend with the increase of n_p , the results are unstable, and the relative errors remain at about 10%. The relative error level of Xie's upper bound is lower than that of the lower bound, but the relative errors increase when n_p exceeds 150. The above results show that the proposed method can obtain more accurate upper and lower bounds of failure probabilities with less discrete cost. When $n_p=120$, the upper and lower bounds of the failure probabilities obtained by the proposed method are 6.5×10^{-4} and **0.157**, respectively, while the relative errors are **0.13%** and **1.36%**.

Table 7. The results of case 4

Method	n_p	\underline{P}_f (Error %)	\overline{P}_f (Error %)	NFc
IMCS	-	6.5×10^{-4}	0.0159	10^6
Xie's	50	8.16×10^{-4} (25.5)	0.0169(6.23)	600
	400	7.10×10^{-4} (9.18)	0.0155(2.58)	6000
The proposed method	750	7.08×10^{-4}(8.91)	0.0154(3.12)	12000
	10	7.43×10^{-4} (14.3)	0.0142(10.7)	4
	20	6.89×10^{-4} (5.94)	0.0151(5.36)	4
	30	6.79×10^{-4} (4.50)	0.0152(4.20)	4
	40	6.77×10^{-4} (4.09)	0.0153(3.55)	4
	50	6.73×10^{-4} (3.55)	0.0154(3.31)	4
	60	6.69×10^{-4} (2.98)	0.0154(2.94)	4
	70	6.67×10^{-4} (2.69)	0.0154(2.92)	4
	80	6.63×10^{-4} (2.05)	0.0155(2.68)	4
	90	6.56×10^{-4} (0.99)	0.0155(2.47)	4
	100	6.51×10^{-4} (0.12)	0.0156(2.21)	4
110	6.52×10^{-4} (0.29)	0.0157(1.40)	4	
	120	6.5×10^{-4}(0.13)	0.157(1.36)	4

In this case, the proposed method calls the function four times. When $n_p=120$, the optimization function dimension is 3×120 , and the calculation time is about 4.28s. The number of

IMCS calculations is 10^6 , and the calculation time is much longer than the proposed method. When $n_p=50$, the NfC of Xie's is $2 \times 2 \times 3 \times 50=600$, representing two optimizations, two iterations, the number of p-box variables and n_p in turn. Because

the conditional failure probability needs to be calculated repeatedly, the calculation time is also higher than that of the proposed method.

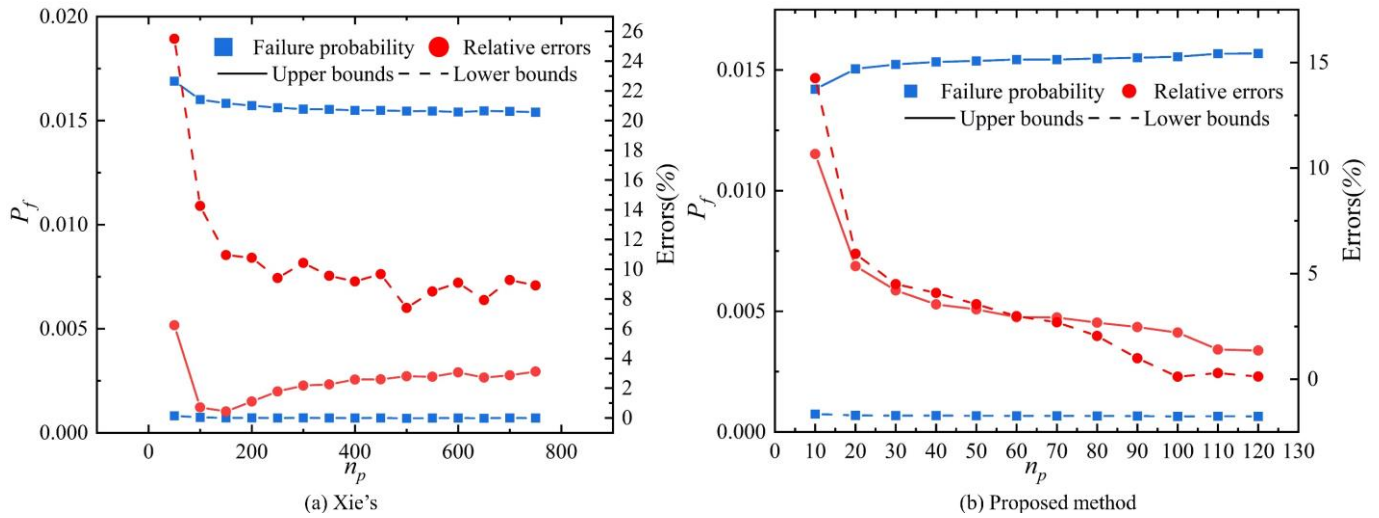


Fig. 17. Failure probability boundaries and relative errors of Case 4.

4.5. Case Study 5: A cantilever tube

The cantilever tube, which is used to consider the influence of variable complexity, is another typical application in engineering. Its schematic diagram is shown in Fig. 18.

There are three external forces F_1 , F_2 , P , and a torsion T exerted on the tube. Because the maximum Von Mises stress σ_{\max} in the tube should be less than 180mpa, the performance function is constructed by

$$\begin{cases} \sigma_x = \frac{P+F_1 \sin(\theta_1)+F_2 \sin(\theta_2)}{A} + \frac{Md}{2I}, \\ \tau_{zx} = \frac{Td}{4I}, \end{cases} \quad (30)$$

where M , A and I are, respectively, calculated by

$$\begin{cases} M = F_1 L_1 \cos(\theta_1) + F_2 L_2 \cos(\theta_2) \\ A = \frac{\pi}{4} [d^2 - (d - 2t)^2] \\ I = \frac{\pi}{64} [d^4 - (d - 2t)^4] \end{cases} \quad (31)$$

The details regarding the random variables and p-box variables can be found in Table 8. The upper and lower bounds of IMCS are 0.0056 and 0.0167, respectively. Set $n_p=500$, the upper and lower bounds calculated by Xie's are 0.00572 and 0.0165. The errors between the two methods are 2.14% and 1.44%. The failure boundaries and relative errors obtained by the proposed method under different n_p are calculated and plotted, as shown in Fig. 19 and Table 11. When $n_p=70$, the results are 0.0052 and 0.0166. With the increase of n_p , the upper and lower bound of the failure probability gradually converges, and the relative errors of the results tend to decrease. When n_p exceeds 30, the errors between the proposed method and the other two methods are less than 4%. The above results can support the view that the proposed method can rapidly converge to the exact boundary at small discrete cost.

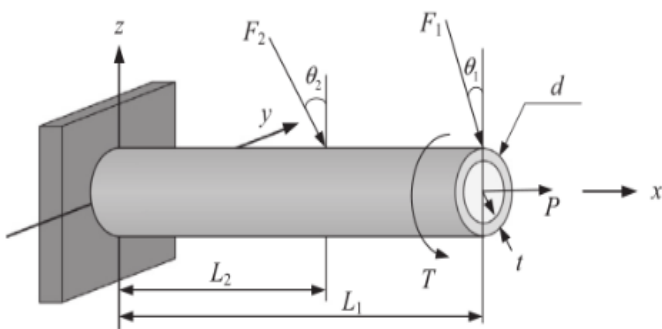


Fig. 18. Schematic diagram of a cantilever tube.

$$G = 180 - \sigma_{\max} \quad (28)$$

and the maximum Von Mises stress σ_{\max} is computed by

$$\sigma \sqrt{\sigma_x^2 + 3\tau_{zx}^2} \quad (29)$$

where σ_x is normal stress and τ_{zx} is torsional stress, and they are calculated by

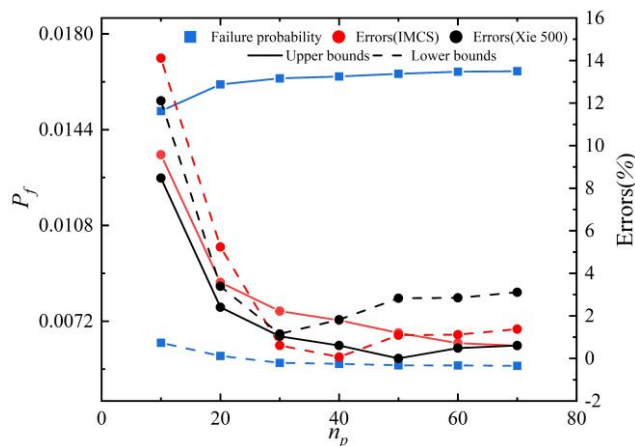


Fig. 19. Failure probability boundaries and relative errors of Case 5.

Table 8. Distribution of variables for a cantilever tube.

Variables	Distribution type	Mean	Standard deviation
t	Normal	5	0.1
d	Normal	42	0.5
$P(N)$	Normal	12000	1200
$T(N \cdot m)$	Normal	90	9
L_2	Uniform	[59.75,60.25]	-
$F_1(N)$	Normal	5000	500
$F_2(N)$	Normal	5000	500
L_1	Normal	[119.5,120.5]	1
θ_1	Normal	[4.9,5.1]	0.9
θ_2	Normal	[9.9,10.1]	1

Table 9. The results of case 5.

Method	n_p	$\underline{P_f}$	Lower Error (IMCS)	Lower Error (Xie 500)	$\overline{P_f}$	Upper Error (IMCS)	Upper Error (Xie 500)	NFc
IMCS	-	0.0056	-	-	0.0167	-	-	10^5
Xie's	500	0.00572	2.14	-	0.0165	1.44	-	9000
	10	0.00639	14.1	12.1	0.0151	9.57	8.48	
	20	0.00589	5.24	3.39	0.0161	3.57	2.40	
The proposed method	30	0.00563	0.611	1.15	0.01633	2.22	1.04	
	40	0.0056	0.0674	1.82	0.0164	1.80	0.606	4
	50	0.00554	1.09	2.83	0.0165	1.20	0	
	60	0.00554	1.12	2.85	0.01658	0.718	0.485	
	70	0.00552	1.38	3.11	0.0166	0.599	0.606	

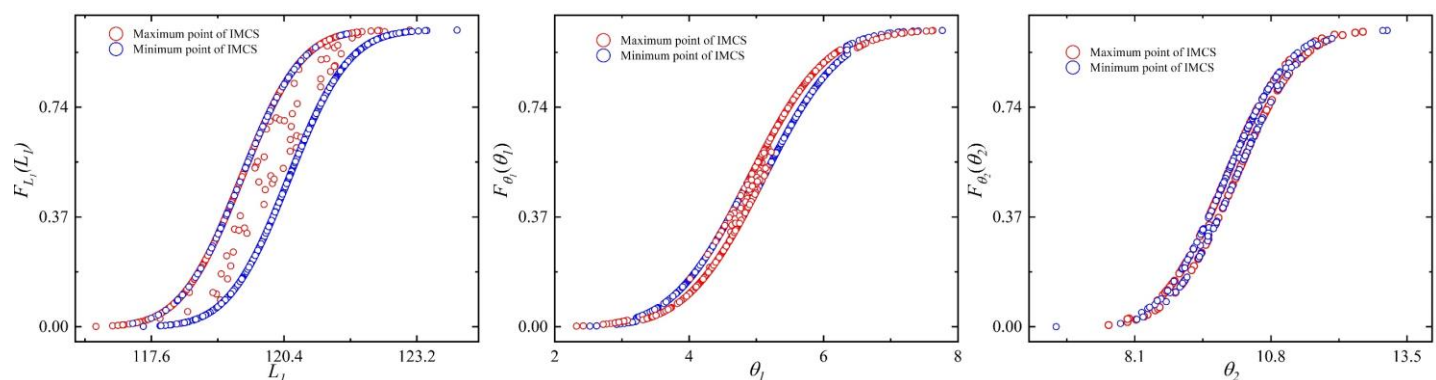


Fig. 20. Extreme points distribution of Case 5.

The distributions of IMCS extreme points are plotted in Fig. 20. It can be seen that the boundaries of the three variables all appear scattered distribution, but the calculation results show that this phenomenon does not affect the calculation results of Case 4. Plot the failure point distribution and the fitting curve in Fig. 21-23. As can be seen from the figure, the failure boundaries of the three variables present a monotonous trend and do not fluctuate. It is concluded that the distribution of failure points is the main factor affecting the calculation result of IMCS. After further observation of the fitting curves, it is

found that the proposed method can better reflect the changing trend of the variable failure boundaries. As shown in **Błąd! Nie można odnaleźć źródła odwołania.**(a), the slope variation interval of the failure points distribution is [9.46,9.67]. The slope variation interval of the curves fitted by the proposed method is [9.51,9.67], and the relative errors are 0.05 and 0. The slope variation interval of the curves fitted by Xie's is [9.352,9.50] with 0.108 and 0.17 errors. The above results show that the fitting curve calculated by the proposed method can describe the characteristics of the variables' failure boundaries

more accurately, so as to obtain a more accurate upper and lower bound of the failure probability.

In addition, in this case, the proposed method has a significant efficiency improvement compared to the other two

methods because the function accesses are always 4 times. The Nfc of IMCS is 10^5 , and that of Xie's is $2 \times 3 \times 3 \times 500 = 9000$, both of which far exceed the proposed method

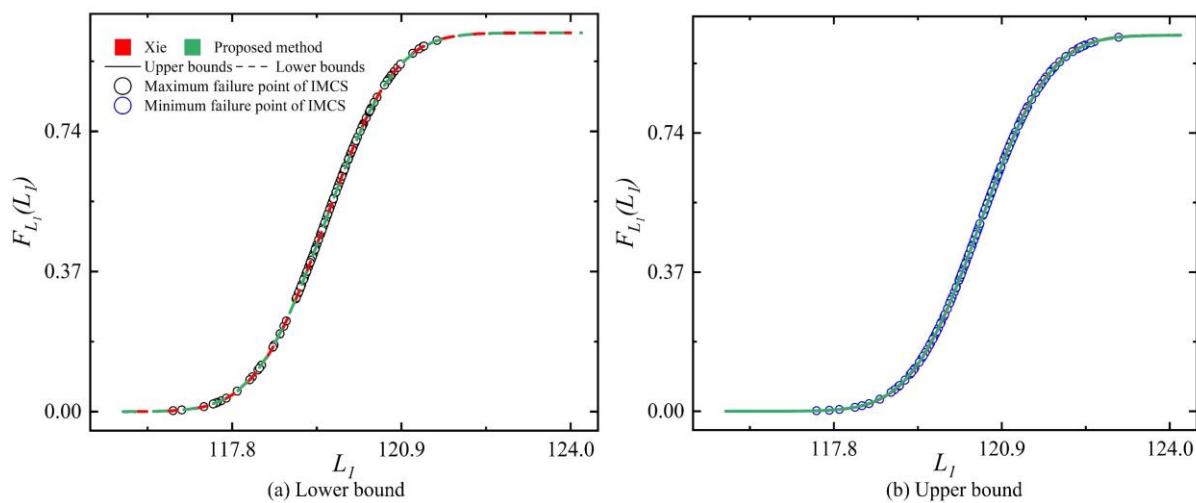


Fig. 21. Failure points distribution and fitting curves of L_1 .

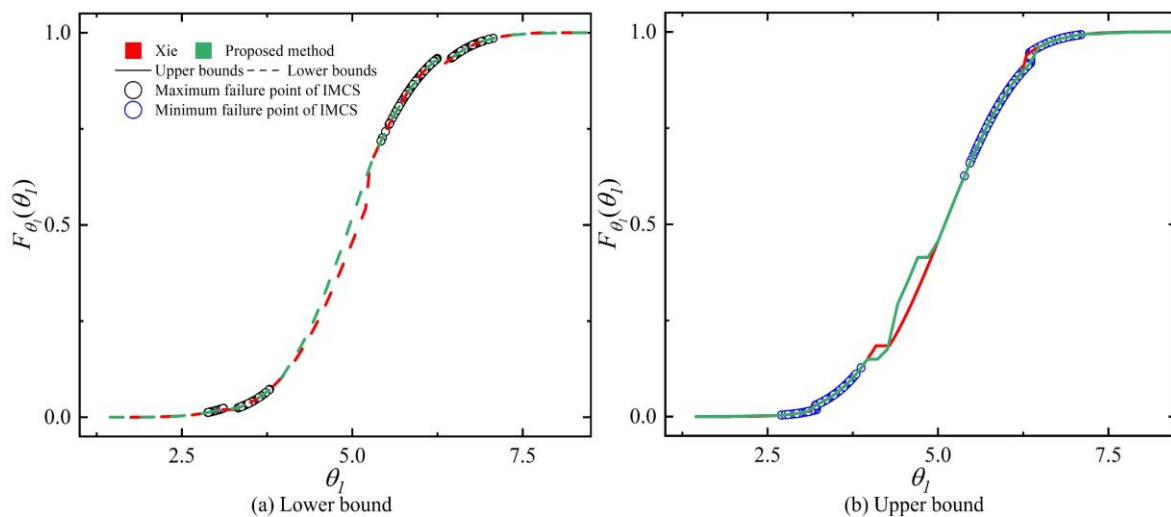


Fig. 22. Failure points distribution and fitting curves of θ_1 .

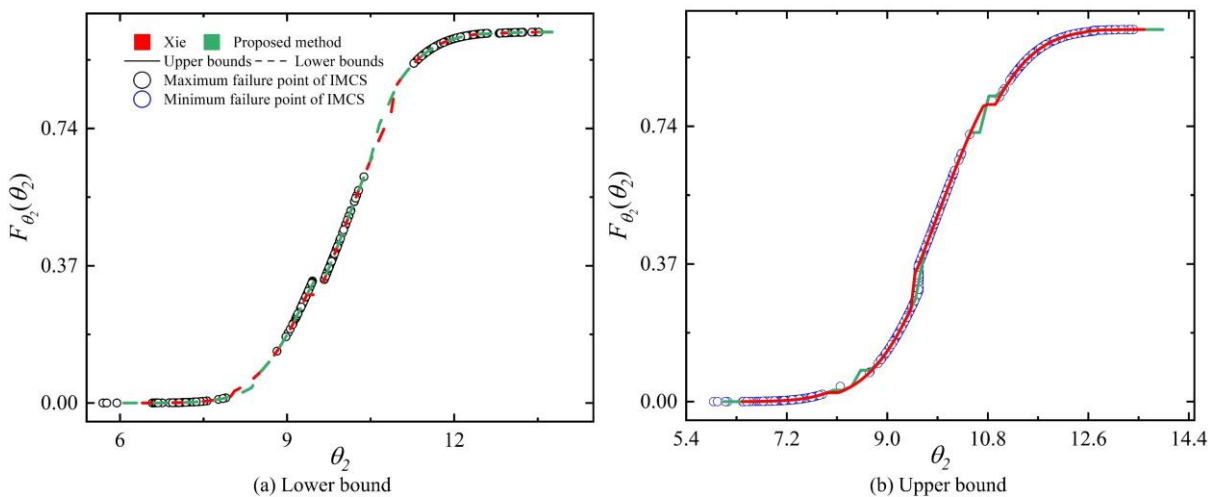


Fig. 23. Failure points distribution and fitting curves of θ_2 .

4.6. Case Study 6: A truss structure

A truss structure is a typical engineering structure, which can be analyzed by the finite element method. As shown in Fig. 24, the truss structure contains 23 bars. Eleven bars are horizontal with random cross section A_1 and Young's moduli E_1 , and the others are sloping with random cross section A_2 and Young's moduli E_2 . Six loads are applied on nodes of horizontal bars. The distribution information is listed in Table 10. When the deflection of node $s(x)$ is larger than a given threshold value of 0.113m, this structure is treated as failed. Therefore, the performance function of the structure is defined as

$$G(x) = 0.113 - |s(x)|. \quad (32)$$

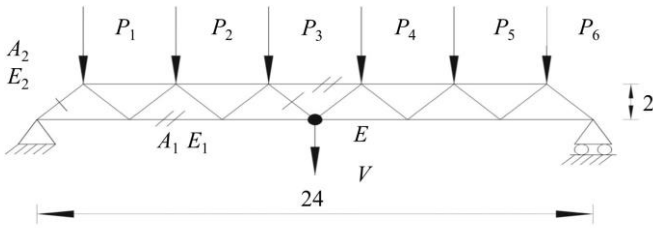


Fig. 24. Schematic diagram of a truss structure.

Table 10. Distribution of variables for a truss structure.

Variables	Distribution type	Mean	Standard deviation
P_1-P_6	Normal	$[5 \times 10^4, 5.5 \times 10^4]$	5×10^3
A_1	Normal	2×10^{-3}	2×10^{-4}
A_2	Normal	1×10^{-3}	1×10^{-4}
E_1	Normal	2.1×10^{11}	2.1×10^{10}
E_2	Normal	2.1×10^{11}	2.1×10^{10}

The sampling number of IMCS is set as 10^5 , and the results are 0.0128 and 0.0523. As shown in Fig. 25, it can be found that the distribution of extreme points shows a monotonous trend. The n_p of Xie's is set as 100, and the results are 0.0127 and 0.0525. As shown in Fig. 26 and Table 11, the failure probability boundaries and relative errors of the proposed method with different n_p are calculated and plotted. The upper and lower bounds of the failure probability calculated by the proposed method are 0.01266 and 0.05227 at $n_p=50$. When n_p exceeds 20, the relative errors are less than 1.5%. Therefore, it can be considered that the results of the proposed method are convergent and can achieve sufficient precision. It can also be concluded from the results that the proposed method has lower

discrete costs and higher computational efficiency than Xie's.

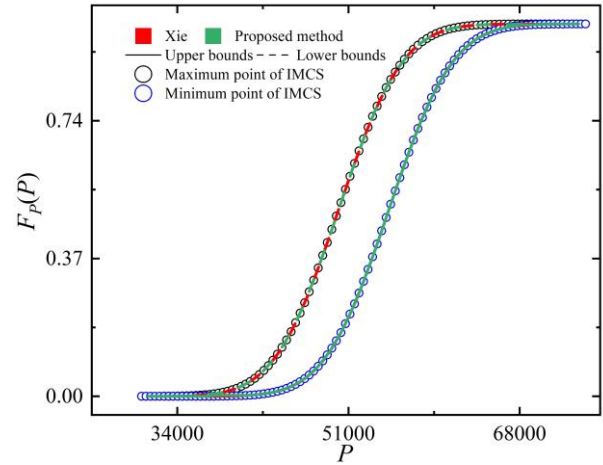


Fig. 25. Points distribution and fitting curves of Case 6.

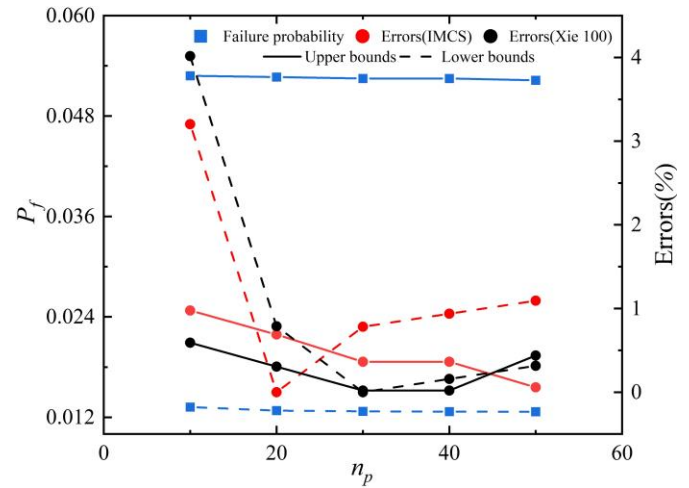


Fig. 26. Failure probability boundaries and relative errors of Case 6.

Table 11. The results of case 6.

Method	n_p	\underline{P}_f (Error %)	\overline{P}_f (Error %)	NFc
IMCS	-	0.0128	0.0523	10^5
Xie's	100	0.0127	0.0525	2400
The proposed method	10	0.01321	0.05281	4
	20	0.01280	0.05266	
	30	0.0127	0.05249	
	40	0.01268	0.05249	
	50	0.01266	0.05227	

4.7. Discussion

The three methods are compared and analyzed according to six cases, and the following conclusions can be drawn:

- (1) The results of six cases indicate that the proposed method can obtain sufficiently accurate results at small dispersion levels. When $n_p=40\sim 50$, the errors between the results of the proposed

method and the results of the IMCS can be kept below 5%. Xie's usually requires more discrete numbers to achieve the same accuracy.

(2) The results of six cases also show that the weight-fitting curves generated by the proposed method accurately depict the main distribution characteristics of IMCS failure points. In Case 4 and Case 5, the proposed method can accurately capture the slope variation trend of the failure boundaries with a relative error of less than 0.1.

(3) According to Case 2 and Case 5, the results show that IMCS exists in the problems described in section 2.2, resulting in a bias in the results. Failure points are the main factor affecting the accuracy of IMCS results. IMCS results tend to be conservative, while the proposed method yields results with higher accuracy.

(4) Compared with Xie's and IMCS, the computational efficiency of the proposed method has been significantly improved in the six cases. This is because the proposed method calls the function and optimizes fewer throughout the calculation process, avoiding the complicated optimization and iteration process.

5. Conclusions

In this paper, a Random-P-box various system failure probability optimization model based on MCS and weight coefficients is constructed, and the reliability of the system is evaluated by the proposed optimization model. The failure samples are mapped from the general random space to the p-box variable space by using the PDFs of the auxiliary input variables and the p-box variable, as well as the important sampling function. During the mapping process, two types of weights are generated: important sampling weights and interval weights. After reconstructing the interval weights using interval

discretization methods, these weights are transformed into variables subject to linear constraints, and a failure probability optimization model is established. The proposed optimization model not only avoids cyclic optimization during the sampling process but also has a complexity independent of the system's performance functions. By solving the optimization equations twice under linear constraints, upper and lower bounds of failure probabilities can be respectively calculated.

By comparing with IMCS and Xie's, the accuracy and efficiency of the proposed method are validated across six different variable dimensions and function complexity cases. The results from each case demonstrate that the proposed method can achieve more accurate results at a lower discretization cost. The weight fitting curves obtained through the proposed method can reflect the main features of the true boundaries of the p-box. Therefore, when dealing with a single p-box variable and monotonic problems, it can ensure sufficient accuracy. For complex monotonicity issues, this method can obtain a more compact failure probability interval, reducing the overestimation of the results. In terms of computational efficiency, the proposed optimization model requires fewer optimization iterations and does not involve calls to the functional functions. Case study results also demonstrate the higher efficiency of the proposed method. In summary, the proposed method is an accurate and effective approach for p-box system reliability assessment, applicable to various computational models. This study has established the foundational model and compared it with the basic model IMCS. To further enhance the computational efficiency and applicability of the model, future work will integrate other optimization algorithms to improve the model solving process and combine it with surrogate models for engineering applications.

References

1. Abdalrdha ZK, Al-Bakry AM, Farhan AK. Analysis of social networks and filtering of Arabic crime tweets based on an intelligent dictionary using a genetic algorithm. *Global Journal of Engineering and Technology Advances*, 2024; 18(02): 177–191. DOI: 10.30574/gjeta.2024.18.2.0033.
2. Ajenjo A, Ardillon E, Chabridon V, Iooss B, Cogan S, Sadoulet-Reboul E. An info-gap framework for robustness assessment of epistemic uncertainty models in hybrid structural reliability analysis. *Structural Safety*, 2022; 96. DOI: 10.1016/j.strusafe.2022.102196.
3. Alhussan AA, Farhan AK, Abdelhamid AA, El-Kenawy ESM, Ibrahim A, Khafaga DS. Optimized ensemble model for wind power forecasting using hybrid whale and dipper-throated optimization algorithms. *Frontiers in Energy Research*, 2023; 11, 1174910. DOI: 10.3389/ferg.2023.1174910.

4. Alvarez DA, Uribe F, Hurtado JE. Estimation of the lower and upper bounds on the probability of failure using subset simulation and random set theory. *Mechanical Systems and Signal Processing*, 2018; 100: 782-801. DOI: 10.1016/j.ymssp.2017.07.040.
5. Certa A, Hopps F, Inghilleri R, La Fata CM. A Dempster-Shafer Theory-based approach to the Failure Mode, Effects and Criticality Analysis (FMECA) under epistemic uncertainty: application to the propulsion system of a fishing vessel. *Reliability Engineering & System Safety*, 2017;159:69-79. DOI:10.1016/j.res.2016.10.018.
6. Dang C, Valdebenito MA, Faes MGR, Wei P, Beer M. Structural reliability analysis: A Bayesian perspective. *Structural Safety*, 2022; 99. DOI: 10.1016/j.strusafe.2022.102259.
7. de Angelis M, Patelli E, Beer M. Advanced Line Sampling for efficient robust reliability analysis. *Structural Safety*, 2015; 52:170-82. DOI: 10.1016/j.strusafe.2014.10.002.
8. Echard B, Gayton N, Lemaire M. AK-MCS: An active learning reliability method combining Kriging and Monte Carlo Simulation. *Structural Safety*, 2011;33:145-54. DOI:10.1016/j.strusafe.2011.01.002.
9. Faes MGR, Daub M, Marelli S, Patelli E, Beer M. Engineering analysis with probability boxes: A review on computational methods. *Structural Safety*, 2021;93. DOI:10.1016/j.strusafe.2021.102092.
10. Guan XL, Melchers REJSS. Effect of response surface parameter variation on structural reliability estimates. *Structural Safety*, 2001; 23(4):429-444.DOI:10.1016/S0167-4730(02)00013-9.
11. Helton JC, Johnson JD, Oberkampf WL. An exploration of alternative approaches to the representation of uncertainty in model predictions. *Reliability Engineering & System Safety*, 2004; 85:39-71. DOI:10.1016/j.res.2004.03.025.
12. Hussain Ali Y, Chinnaperumal S, Marappan R, Raju SK, Sadiq AT, Farhan AK, Srinivasan P. Multi-Layered Non-Local Bayes Model for Lung Cancer Early Diagnosis Prediction with the Internet of Medical Things. *Bioengineering*. 2023; 10(2):138. DOI: 10.3390/bioengineering10020138.
13. Hussain Ali Y, SabuChooralil V, Balasubramanian K, Manyam RR, Kidambi Raju S, T. Sadiq A, Farhan AK. Optimization system based on convolutional neural network and internet of medical things for early diagnosis of lung cancer. *Bioengineering*, 2023; 10:320. DOI: 10.3390/bioengineering10030320.
14. Kang Z, Zhang W. Construction and application of an ellipsoidal convex model using a semi-definite programming formulation from measured data. *Computer Methods in Applied Mechanics and Engineering*, 2016; 300: 461-89. DOI: 10.1016/j.cma.2015.11.025.
15. Kamal ZA, Kadhim A. Generating dynamic S-BOX based on Particle Swarm Optimization and Chaos Theory for AES. *IRAQI JOURNAL OF SCIENCE*, 2018; 59(3c):1733-1745. DOI:10.24996/ijs.2018.59.3c.18.
16. Li JW, Jiang C, Ni BY. An Efficient Uncertainty Propagation Analysis Method for Problems Involving Non-Parameterized Probability-Boxes. *Journal of Mechanical Design*, 2021;143. DOI:10.1115/1.4050559.
17. Liang H , Mi J , Bai L , et al. Imprecise sensitivity analysis of system reliability based on the Bayesian network and probability box. *Eksplatacja i Niezawodność – Maintenance and Reliability*, 2020; 22(3): 508-519. DOI:10.17531/EIN.2020.3.14.
18. Liu HB, Jiang C, Jia XY, Long XY, Zhang Z, Guan FJ. A new uncertainty propagation method for problems with parameterized probability-boxes. *Reliability Engineering & System Safety*, 2018;172:64-73. DOI:10.1016/j.res.2017.12.004.
19. Liu HB, Jiang C, Liu J, Mao JZ. Uncertainty propagation analysis using sparse grid technique and saddlepoint approximation based on parameterized p-box representation. *Structural and Multidisciplinary Optimization*, 2018; 59: 61-74. DOI: 10.1007/s00158-018-2049-5.
20. Liu HB, Jiang C, Xiao Z. Efficient uncertainty propagation for parameterized p-box using sparse-decomposition-based polynomial chaos expansion. *Mechanical Systems and Signal Processing*, 2020; 138. DOI:10.1016/j.ymssp.2019.106589.
21. Liu X, Kuang Z, Yin L, Hu L. Structural reliability analysis based on probability and probability box hybrid model. *Structural Safety*, 2017;68:73-84. DOI:10.1016/j.strusafe.2017.06.002
22. Liu X, Li T, Zhou Z, Hu L. An efficient multi-objective reliability-based design optimization method for structure based on probability and interval hybrid model. *Computer Methods in Applied Mechanics and Engineering*, 2022; 392. DOI: 10.1016/j.cma.2022.114682.
23. Meng Z, Zhao J, Chen G, Yang D. Hybrid uncertainty propagation and reliability analysis using direct probability integral method and exponential convex model. *Reliability Engineering & System Safety*, 2022; 228. DOI: 10.1016/j.res.2022.108803.
24. Montes I, Destercke S. On extreme points of p-boxes and belief functions. *Annals of Mathematics and Artificial Intelligence*, 2017; 81:405-28. DOI:10.1007/978-3-319-42972-4_45.

25. Oberkampf W L, Helton J C, Joslyn C A, et al. Challenge problems: uncertainty in system response given uncertain parameters. *Reliability Engineering & System Safety*, 2004; 85(1-3):11-19. DOI:10.1016/j.ress.2004.03.002.
26. Pedroni N, Zio E, Apostolakis GEJRE, Safety S. Comparison of bootstrapped artificial neural networks and quadratic response surfaces for the estimation of the functional failure probability of a thermal-hydraulic passive system. *Reliability Engineering & System Safety*, 2012; 95(4):386-395. DOI:10.1016/j.ress.2009.11.009.
27. Rekuć SJ, Aughenbaugh JM, Bruns M, Paredis C. Eliminating Design Alternatives Based on Imprecise Information. *Sae Technical Papers*, 2006. DOI:10.4271/2006-01-0272.
28. Roy A, Chakraborty S. Support vector machine in structural reliability analysis: A review. *Reliability Engineering & System Safety*, 2023; 233. DOI: 10.1016/j.ress.2023.109126.
29. Schöbi R, Sudret B. Structural reliability analysis for p-boxes using multi-level meta-models. *Probabilistic Engineering Mechanics*, 2017;48:27-38. DOI:10.1016/j.probengmech.2017.04.001.
30. Schobi R, Sudret B. Global sensitivity analysis in the context of imprecise probabilities (p-boxes) using sparse polynomial chaos expansions. *Reliability Engineering & System Safety*, 2019; 187(JUL.):129-141. DOI:10.1016/j.ress.2018.11.021.
31. Song Y, Mi J, Cheng Y, Bai L, Chen K. A Dependency Bounds Analysis Method for Reliability Assessment of Complex System with Hybrid Uncertainty. *Reliability Engineering & System Safety*, 2020; 204: 107119. DOI: 10.1016/j.ress.2020.107119.
32. Soundappan P, Nikolaidis E, Haftka RT, Grandhi R, Canfield R. Comparison of evidence theory and Bayesian theory for uncertainty modeling. *Reliability Engineering & System Safety*, 2004; 85:295-311. DOI:10.1016/j.ress.2004.03.018.
33. Xiao N-C, Yuan K, Zhou C. Adaptive kriging-based efficient reliability method for structural systems with multiple failure modes and mixed variables. *Computer Methods in Applied Mechanics and Engineering*, 2020; 359. DOI: 10.1016/j.cma.2019.112649.
34. Xiao T, Park C, Lin C, Ouyang L, Ma Y. Hybrid reliability analysis with incomplete interval data based on adaptive Kriging. *Reliability Engineering & System Safety*, 2023; 237. DOI: 10.1016/j.ress.2023.109362.
35. Xie J, Tian Z, Zhi P, et al. Reliability analysis method of coupling optimal importance sampling density and multi-fidelity Kriging model. *Eksploatacja i Niezawodność – Maintenance and Reliability*, 2023; 25 (2). DOI: 10.17531/ein/161893.
36. Xie H, Li J, Liao D. A new structural reliability analysis method under non-parameterized probability box variables. *Structural and Multidisciplinary Optimization*, 2022; 65(11):1-10. DOI:10.1007/s00158-022-03408-5.
37. Yang X, Liu Y, Zhang Y, Yue Z. Hybrid reliability analysis with both random and probability-box variables. *Acta Mechanica*, 2014;226:1341-57. DOI:10.1007/s00707-014-1252-8.
38. Yang X, Wang T, Li J, Chen Z. Bounds approximation of limit-state surface based on active learning Kriging model with truncated candidate region for random-interval hybrid reliability analysis. *International Journal for Numerical Methods in Engineering*, 2019; 121:1345-66. DOI:10.1002/nme.6269.
39. Yan Y, Zhou J, Yin Y, Nie H, Wei X, Liang T. Reliability Estimation of Retraction Mechanism Kinematic Accuracy under Small Sample. *Eksploatacja i Niezawodność – Maintenance and Reliability*, 2023. DOI:10.17531/ein/174777.
40. Yin H, Yu D, Xia B. Reliability-based topology optimization for structures using fuzzy set model. *Computer Methods in Applied Mechanics and Engineering*, 2018; 333:197-217. DOI: 10.1016/j.cma.2018.01.019.
41. Yun W, Lu Z, Feng K, Jiang X. A novel step-wise AK-MCS method for efficient estimation of fuzzy failure probability under probability inputs and fuzzy state assumption. *Engineering Structures*, 2019; 183: 340-50. DOI: 10.1016/j.engstruct.2019.01.020.
42. Zhan H, Xiao NC, Ji Y. An adaptive parallel learning dependent Kriging model for small failure probability problems. *Reliability Engineering & System Safety*, 2022; 222:108403-. DOI:10.1016/j.ress.2022.108403.
43. Zhang H. Interval importance sampling method for finite element-based structural reliability assessment under parameter uncertainties. *Structural Safety*, 2012;38:1-10. DOI:10.1016/j.strusafe.2012.01.003.
44. Zhang H, Dai H, Beer M, Wang W. Structural reliability analysis on the basis of small samples: An interval quasi-Monte Carlo method. *Mechanical Systems and Signal Processing*, 2013;37:137-51. DOI:10.1016/j.ymssp.2012.03.001.
45. Zhang H, Mullen RL, Muhanna RL. Interval Monte Carlo methods for structural reliability. *Structural Safety*, 2010; 32:183-90. DOI:10.1016/j.strusafe.2010.01.001.
46. Zhang J, Xiao M, Gao L, Chu S. A bounding-limit-state-surface-based active learning Kriging method for hybrid reliability analysis under

- random and probability-box variables. *Mechanical Systems and Signal Processing*, 2019; 134. DOI:10.1016/j.ymsp.2019.106310.
47. Zhang K , Chen N , Liu J , Yin S, Beer M. An efficient meta-model-based method for uncertainty propagation problems involving non-parameterized probability-boxes. *Reliability Engineering & System Safety*, 2023. DOI: 10.1016/j.res.2023.109477.
48. Zhang L ,Zhang J ,Zhai H , et al. A new assessment method of mechanism reliability based on chance measure under fuzzy and random uncertainties. *Eksploracja i Niezawodność – Maintenance and Reliability*, 2018; 20(2):219-228. DOI:10.17531/ein.2018.2.06.
49. Zhao X, Qunwang Z, Zhe Z, Wenqi B, Haibo L. A collaborative quasi-Monte Carlo uncertainty propagation analysis method for multiple types of epistemic uncertainty quantified by probability boxes. *Structural and Multidisciplinary Optimization*, 2023; 66(5). DOI:10.1007/s00158-023-03564-2.